

INDREK MUST

Ionic and capacitive electroactive laminates
with carbonaceous electrodes as sensors
and energy harvesters



DISSERTATIONES TECHNOLOGIAE UNIVERSITATIS TARTUENSIS

17

INDREK MUST

Ionic and capacitive electroactive laminates
with carbonaceous electrodes as sensors and
energy harvesters



The study was carried out at the Institute of Technology, Faculty of Science and Technology, University of Tartu, Estonia.

The Dissertation was admitted on August 14, 2014 in partial fulfillment of the requirements for the degree of Doctor of Philosophy (Physical Engineering) and allowed for defense by the Scientific Council of the Institute of Technology of the Faculty of Science and Technology of the University of Tartu.

Supervisors: Dr. Andres Punning, University of Tartu
Prof. Alvo Aabloo, University of Tartu

Opponent: Jun.-Prof. Dr. Volker Presser, INM – Leibniz Institute for
New Materials & Saarland University, Germany

Defense: Auditorium 121, Nooruse 1, Tartu, Estonia on September 29,
2014 at 15:00.

Publication of this thesis is granted by the Institute of Technology, Faculty of Science and Technology, University of Tartu and by the Estonian Doctoral School in Information and Communication Technology created under the auspices of European Social Fund.



ISSN 2228-0855
ISBN 978-9949-32-658-7 (print)
ISBN 978-9949-32-659-4 (pdf)

Copyright: Indrek Must, 2014

University of Tartu Press
www.tyk.ee

CONTENTS

LIST OF ORIGINAL PUBLICATIONS	7
LIST OF ABBREVIATIONS AND NOTATIONS	8
1. IONIC AND CAPACITIVE ELECTROACTIVE LAMINATES	9
1.1 Introduction	9
1.2 State-of-the-art applications for IEAP	10
1.2.1 IEAP as a supercapacitor	10
1.2.2 IEAP as an actuator	11
1.2.3 IEAP as a motion sensor	13
1.2.4 IEAP for sensing stimuli other than mechanical	15
1.2.5 IEAP as an energy harvester	16
1.3 Humidity-sensitivity of IEAP	16
2. FROM SENSORS TO ENERGY HARVESTERS	18
2.1 Energy harvesting in micro-scale	18
2.2 The current role of supercapacitors in energy harvesting	19
2.3 Ambient humidity as an energy source	20
3. RESEARCH MOTIVATION	22
4. SENSORIAL PROPERTIES OF IEAP	24
4.1 Working principle	24
4.1.1 Mechanoelectrical transduction	25
4.1.2 Hydroelectrical transduction	26
4.2 Considerations for design of IEAP sensors	26
4.3 Selection of materials	27
4.3.1 CDC as an electrode material	27
4.3.2 IL as an electrolyte	29
4.3.3 Polymeric separator and binder	31
4.4 The IEAP laminates investigated in this work	33
5. IEAP AS A MOTION SENSOR	36
5.1 Characterization of IEAP motion sensors by homogeneous bending	36
5.1.1 Rigs for homogeneous bending of the IEAP	37
5.2 Transient response of IEAP Type II	38
5.2.1 Experimental set-up	38
5.2.2 Results	38
5.3 Motion-sensing properties of IEAP Type I	40
5.3.1 Experiment set-up	40
5.3.2 Frequency-response of IEAP Type I	42
5.4 Working principle of IEAP motion sensor	44
5.5 Characteristics of the carbon-based IEAP motion sensors	46

6. THE INFLUENCE OF AMBIENT HUMIDITY ON THE ELECTRICAL PARAMETERS OF IEAP	49
6.1 Introduction	49
6.2 Experimental	49
6.3 Electrical impedance of IEAP at different relative humidities	50
6.4 Electrical equivalent circuit for an IEAP	51
6.5 Impedance analysis results and discussion	52
7. IEAP AS A HYGROELECTRICAL SENSOR	55
7.1 Set-up for measurement of hygroelectrical properties	56
7.2 Transient response to humidity gradient	57
7.2.1 Open-circuit voltage	57
7.2.2 Cyclic stability	62
8. IEAP AS AN ENERGY HARVESTER	63
8.1 IEAP for hygroelectrical energy harvesting	63
9. CONCLUSIONS	65
10. SUMMARY IN ESTONIAN	67
11. REFERENCES	69
ACKNOWLEDGEMENTS	79
PUBLICATIONS	81
CURRICULUM VITAE	129

LIST OF ORIGINAL PUBLICATIONS

This thesis is based on four full papers, published in peer-reviewed journals indexed by Thomson Reuters Web of Science. The papers below are listed in order of appearance in the main article of this thesis.

- I. Must, I., Kaasik, F., Põldsalu, I., Johanson, U., Punning, A. & Aabloo, A. (2012) **A carbide-derived carbon laminate used as a mechano-electrical sensor**, *Carbon*, **50**, 535–541.
- II. Must, I., Anton, M., Viidalepp, E., Põldsalu, I., Punning, A. & Aabloo, A. (2013) **Mechano-electrical impedance of a carbide-derived carbon-based laminate motion sensor at large bending deflections**, *Smart Materials and Structures*, **22**, 104015.
- III. Must, I., Vunder, V., Kaasik, F., Põldsalu, I., Johanson, U., Punning, A. & Aabloo, A. (2014) **Ionic liquid-based actuators working in air: the effect of ambient humidity**, *Sensors & Actuators: B. Chemical*, **202**, 114–122.¹
- IV. Must, I., Johanson, U., Kaasik, F., Põldsalu, I., Punning, A. & Aabloo, A. (2013) **Charging supercapacitor-like laminate with ambient moisture: from humidity sensor to energy harvester**, *Physical Chemistry Chemical Physics*, **15**, 9605–9614.

AUTHOR'S CONTRIBUTION

- Paper I:** Author constructed the measurement set-up, performed all experimentation and data processing, and was responsible for writing the paper.
- Paper II:** Author performed all measurements and data processing, and was responsible for writing the paper. Author supervised E. Viidalepp in the construction of the used measurement device.
- Paper III:** Author collaborated in preparation of the measurement apparatus and conduction of the experiments, conducted all data analysis, and was responsible for writing the paper.
- Paper IV:** Author initiated the study, prepared the measurement apparatus, conducted all measurements and data analysis, and was responsible for writing the paper.

¹ Only the results on impedance measurements are covered in this thesis; the effect of humidity on actuation properties is not in the scope of this thesis.

LIST OF ABBREVIATIONS AND NOTATIONS

b	Width of IEAP laminate
B ₄ C-CDC	Boron carbide-derived carbon
CDC	Carbide-derived carbon
CNT	Carbon nanotube
CPE	Constant phase element
CPE_p	Constant phase element connected in parallel
CPE_p-P	P-parameter of constant phase element connected in parallel
CPE_p-T	T-parameter of constant phase element connected in parallel
DAQ	Data acquisition
DMAc	N,N-dimethylacetamide
EMI ⁺	1-ethyl-3-methylimidazolium cation
EMIBF ₄	1-ethyl-3-methylimidazolium tetrafluoroborate
EMITFS	1-ethyl-3-methylimidazolium trifluoromethanesulfonate
IEAP	Ionic electroactive polymer
IL	Ionic liquid
I_{pp}	Peak-to-peak current
IPMC	Ionic polymer-metal composite
MEMS	Microelectromechanical systems
MP	4-methyl-2-pentanone
PC	Propylene carbonate
PEDOT:PSS	Poly(3,4-ethylenedioxythiophene) poly(styrene sulfonate)
PTFE	Polytetrafluoroethylene
PVdF-HFP	Polyvinylidene fluoride-co-hexafluoropropylene
RH	Relative humidity
R_c	Current-measuring (shunt) resistor
R_p	Parallel resistance
R_s	Series resistance
SWCNT	Single-walled carbon nanotube
TiC-CDC	Titanium carbide-derived carbon
TFS ⁻	Trifluoromethanesulfonate anion
t_ω	Frequency-dependent parameter of Warburg impedance
U_{pp}	Peak-to-peak voltage
W_c	Exponent parameter of Warburg impedance
W_r	Proportional parameter of Warburg impedance
WSN	Wireless sensor network
$ Z $	Impedance modulus
Z_w	Warburg impedance
ω	Angular frequency
ω_t	Characteristic frequency of Warburg impedance

I. IONIC AND CAPACITIVE ELECTROACTIVE LAMINATES

I.1 Introduction

The rapidly growing fields of soft robotics and flexible electronics are in demand of compatible soft stimulus-responsive materials [1,2]. The shift from conventional, *rigid* robotics and semiconductor-based electronics, which both engage electron transport and magnetic fields in their working principle, towards fully or partially soft devices also implies fundamentally different device configurations and their underlying physical working principles. Soft devices often mimic sensation and actuation mechanisms commonly found in the nature – they engage ionic currents and rely on the counteraction between electronically and ionically conductive materials [3,4]. The constitutive units in soft robotics and flexible electronics are often multifunctional; *i.e.* the same subsystem can perform simultaneously or intermittently multiple tasks in a system. For example, a structural member of a soft robot’s body can also act as a sensor, an actuator, or even an energy storage unit.

The thesis at hand explores the electroactive properties of one specific class of materials, targeted for use in soft robotics and flexible electronics applications. This material is referred to as an ionic electroactive polymer (IEAP). An IEAP is a soft, thin, symmetrical laminate, which consists of a microporous polymeric membrane in-between two microporous electrodes with a high specific surface area. The membrane and the electrodes are swollen by an appropriate electrolyte. The electrodes are both electronically and ionically conductive, whereas the membrane conducts only ions.

The definition for the IEAP given above applies for a number of different devices in the soft robotics and flexible electronics domains. The applications of particular interest for IEAP are:

- Flexible supercapacitors
- Electromechanical actuators
- Motion sensors
- Energy harvesters

Similar materials are used in construction of devices for any of the applications listed above. These devices are distinguished mainly by their particular geometric configuration and optimization of the materials. As an example, if a particular IEAP, regardless of its function, is expected to be exposed to ambient air and to be operable at room temperature, then the electrolyte for this IEAP is prospectively selected from the class of room-temperature ionic liquids (ILs). On the contrary, a solvent-based electrolyte is, as a rule, a more reasonable choice for a hermetically sealed IEAP.

The electrode materials considered for IEAP can be generally divided into two major categories: the materials undergoing Faradaic charge-transfer reactions during operation, or non-Faradaic materials, which do not undergo charge-transfer reactions. The work at hand focuses on the IEAPs with non-

Faradaic, carbonaceous electrodes. Microporous carbon is one of the most widely used electrode material for IEAP due to its electrochemical inertness and a wide diversity of available forms, ranging from powders to fibers, cloths, monoliths, nanoscale structures, etc. [5].

In all of the abovementioned applications for IEAP, the ion transport properties between the electrodes [6] and the interaction between the ionic species and the electronically conductive electrodes are of particular importance. A good match between the porosity distribution of the electrode material and the effective sizes of the ions in the electrolyte must be made to achieve a device with tailored properties. The properties of IEAP can be tuned by the proper choice of electrolyte and by changing the precursors or synthesis process parameters of the carbonaceous electrode materials [5,7]. In addition, the choice of polymeric separator and binder also influences the ionic conduction properties and, in turn, the electroactive properties of IEAP [6,8].

Up to the present, the research on IEAP has been primarily distinguished by the expected role – either as a supercapacitor, an actuator, or a sensor – of the particular type of IEAP in a mechatronic system. The state-of-the-art of the research on IEAP, categorized by their projected primary application, is reviewed in the next subsection.

1.2 State-of-the-art applications for IEAP

1.2.1 IEAP as a supercapacitor

Supercapacitors store electric energy by reversible electrostatic accumulation of mobile ions on the surface of the electrodes with high specific surface area. Supercapacitors are commonly characterized by their high current and power density, but their energy density is lower compared to batteries [5]. A supercapacitor was first constructed by Becker *et al.* from General Electric Co. in 1957 [9] and commercialized already in 1978 by NEC [10]. Conventional supercapacitors are sealed systems, which involve volatile organic electrolytes. The commonly used electrolytes for the supercapacitors are acetonitrile and propylene carbonate, containing tetraethylammonium tetrafluoroborate salt. ILs are promising electrolytes for the supercapacitors especially due to their high electrochemical window (>4 V); however, only in water-free conditions [11]. What is more, supercapacitors with IL as an electrolyte typically yield lower energy density and higher relaxation times compared to the supercapacitors with organic solvents as an electrolyte [12].

Starting from the year 2008 (based on the number of published papers according to the ISI Web of Knowledge), the development of flexible, creasable, and stretchable supercapacitors has been an accelerating trend. The stimulus for making the supercapacitors more flexible is the demand for power storage elements that are compatible with flexible and wearable electronic devices [13–15]. Unlike the conventional, sealed supercapacitors, which serve only as monofunctional energy storage units, flexible supercapacitors can also

perform as structural components, therefore reducing the weight and volume of portable electronics [16–19]. Flexible supercapacitors are often constructed as thin laminates, but supercapacitors in the form of weavable fibers have recently become increasingly popular [14,20].

The state-of-the-art flexible supercapacitor prototypes are, as a rule, characterized and hence expected to operate in a totally water-free environment. Complete sealing of these devices against water absorption is presumed, by default, in a real-world device. Complete sealing becomes increasingly difficult to achieve, especially in consideration of some recent reports on supercapacitors capable of undergoing strain exceeding 100% [21]. A large number of prospective fields of application for the flexible supercapacitors presume their ability for long-term operation in air, possibly being directly exposed to air. ILs have also been considered as electrolytes for the flexible supercapacitors also due to their nonvolatility [22,23]. However, the research on in-air-operable supercapacitors, or even general characterization of supercapacitors exposed to ambient air, has not yet found significant interest in the scientific literature.

The supercapacitors are attractive also for their use in micro-scale devices; therefore, methods for integrating supercapacitors with the manufacturing processes used in fabrication of contemporary microelectronics and micro-electromechanical systems (MEMS) are sought. Contrarily to the conventional supercapacitors, which are typically characterized by their gravimetric specific capacitance in respect to the mass of their electrode material, the most relevant criterion for the micro-supercapacitors is their areal energy and power density, as the mass of their active electrode material, compared to the total mass of the device, is often negligibly small. Another reason is that the capacitance of a single electrode does not always scale up with its thickness [24].

1.2.2 IEAP as an actuator

In 1992, Oguro *et al.*, Shahinpoor *et al.*, and Sadeghipour *et al.* almost simultaneously constructed an electromechanical actuator that had fluoropolymer-copolymer with covalently bonded anionic moieties as a membrane [25]. The ionic polymer membrane was coated with compliant, electronically conductive, noble metal electrodes; thus, the resulting IEAP material is often called as an ionic polymer-metal composite (IPMC). The working principle of an IPMC is straightforward – the mobile cations in the ionic polymer membrane, together with their water solvation shells, are drawn towards negatively charged electrode by applying electric potential difference between the metal electrodes. The resulting pressure difference between the opposite sides of the ionic polymer membrane emerges volumetric effects and causes bending of the IPMC [25,26]. The large dependence on its hydration level makes in-air use of the solvent-based IEAPs complicated.

Conjugated polymers – polymers with electronically conductive backbone due to π -conjugation – are perspective alternative electrode materials for ionic actuators, which have been developed since the early 1990s [27]. Volumetric

changes in the conductive polymer electrodes are obtained by entrance or expulsion of mobile counter-ions, driven by reversible electrochemical oxidation or reduction (that is, Faradaic charge-transfer reactions) of the conjugated polymer [28].

Carbon was conceived as a perspective electrode material for IEAP actuators one decade later – in 1999, despite of the fact that carbon-based supercapacitors were already commercially available even before the 1990s. In 1999, Baughman *et al.* demonstrated electrically induced actuation of a three-layered laminate with single-walled carbon nanotube electrodes in an aqueous electrolyte [29]. The bending phenomenon was explained by quantum chemical effects in the carbon, resulting in elongation of the single-walled nanotubes. In the beginning of the 2000s, IL was conceived as a promising electrolyte to construct electrochemical devices operable directly in air. Lu *et al.* demonstrated IL as a suitable electrolyte for conductive polymer-based IEAP actuators in 2002 [30]. The next breakthrough in the world of IEAPs was the discovery of ‘bucky gel’ – a highly viscous composite of carbon nanotubes and IL – by Fukushima *et al.* in 2003 [31]. Soon after that, Fukushima *et al.* presented *dry* actuators with ‘bucky gel’ electrodes [32]. The mechanical properties of the ‘bucky gel’ electrodes enable construction of electrodes without any additional polymer as a binder [33]. Additionally, high electric conductivity of the single-walled carbon nanotubes in the electrodes was sufficient to omit metal current collectors. Subsequently, electrically induced volumetric effects were demonstrated on various forms of activated carbons, such as carbide-derived carbon [34], carbon aerogel [35], and graphene [36]. In 2013, electrically induced anisotropic linear strain as much as 56% was demonstrated on an IEAP with aligned nanoporous microwave-exfoliated graphite oxide electrodes [37].

The IEAP actuators with carbonaceous electrodes are characterized by large value of electric capacitance; this is not surprising, concerning their intrinsic similarity to the supercapacitors. The gravimetric capacitance per carbon content of an IEAP actuator with IL electrolyte – up to 120 F g^{-1} [38,39] – is in the same order of magnitude with supercapacitors. As a comparison, the commercial supercapacitors with activated carbon electrodes yield 100 F g^{-1} in organic, 200 F g^{-1} in aqueous [40], and 125 F g^{-1} in IL electrolytes [12]. Generally, the IEAPs that are optimized for actuation have significantly lower cyclic energy-storage efficiency (84% [39]).

IEAP actuators are often constructed as cantilevers undergoing bending motion [29,32], but the linear length change of individual electrodes [37] or the change in the thickness of the whole laminate [34] has also been employed.

The response speed of IEAP actuators is limited by diffusion of the ions and solvents within the IEAP laminate; therefore, IEAP actuators reveal their unique capability especially at the lower end of the size scale. IEAP micro-actuators as small as under $50 \mu\text{m}$ in length [41] and $6 \mu\text{m}$ in thickness [42] have been fabricated. The conventional, electromagnetic induction-based actuators become increasingly difficult to fabricate in sub-centimeter size scale. Instead, IEAP

actuators can be prepared in small scale, possibly using existing printing technologies.

Simple control over bipolar actuation by only controlling the electric potential or current applied between the electrodes, large displacement amplitudes in the cantilevered mode, low elastic modulus, metal-free construction, and, most importantly, drastically lower working voltages compared to the piezoelectric or dielectric elastomer actuators, have motivated an extensive development of IEAP actuators.

1.2.3 IEAP as a motion sensor

It is known that many types of energy conversion devices work in either direction. For example, a piezoelectric pressure sensor that generates voltage in response to a mechanical input can be operated as well as an actuator by applying voltage from an external power source. There exists also a counter-effect in IEAP actuators – electric potential difference, or electric current, can be formed between its electrodes as a result of mechanical stimulus.

The shape of an IEAP in a cantilever configuration changes when electric charge is injected to it from an external power source, and the same IEAP generates electric charge, when the cantilever is bent with an external force. Mechano-electrical transduction has been previously comprehensively studied on the IEAPs with inert metal electrodes (*i.e.* IPMCs) [43]. Mechano-electrical transduction of the IEAPs with carbonaceous electrodes has previously attracted only occasional interest. A variety of proposed IEAP motion sensor configurations, as well as the status of the research on motion-sensing parameters of different types of IEAPs, is covered in the next sections.

a. Motion sensor configurations

IEAP motion sensors often share construction and optimization principles with IEAP actuators. In a number of possible applications for IEAP, both actuation and sensing property is required. It can be advantageous, if the same IEAP laminate is operable, either intermittently or simultaneously, as an actuator or a motion sensor, as currently required. From the perspective of manufacturing of IEAP-based devices, it is definitely more convenient to fabricate the actuators and sensors in a single process. It has been demonstrated on different types of IEAPs that an IEAP, optimized for actuation, also functions well as a motion sensor [44,45].

An actuator that can sense mechanical perturbations during actuation via the same wires the actuator is driven through, without any additional sensors, has been demonstrated on the IEAPs driven by Faradaic reactions [46]. Self-sensing of the IEAPs with non-Faradaic, carbon-based electrodes is possible by measuring the impedance of the individual electrodes [47]. Another approach is patterning of the electrodes of an IEAP laminate into separate parts that are responsible either for actuation or for sensing [45,48]. However, the most common and potentially the most practical configuration for an IEAP as a

motion sensor involves measurement of voltage or electric current between the IEAP electrodes.

b. IPMCs as motion sensors

Mechanoelectrical transduction of the IPMCs was conceived almost simultaneously with its actuation property [49]. However, the actual mechanism governing the sensing phenomenon of the IPMCs is still under debate [50,51]. Consequently, as its working mechanism is not fully understood, optimization of the IPMC motion sensors is currently done by trial-and-error.

The major competing explanations for the charge-generation phenomenon are as follows. (a) The pressure-driven flow of diluent in the ionic polymer membrane because of mechanical bending creates an effective dipole in the pressure gradient direction due to orientation of the cations and anions in the ionic polymer clusters [52]. (b) The pressure difference, exerted by mechanical bending, causes a flow of solvent together with the mobile cations, therefore creating a net charge imbalance [53]. (c) More recently, it has been suggested that the electric double-layer at the electrode-electrolyte boundary is disrupted by a flow of electrolyte and solvent, giving a rise to the streaming potential [50,51,54].

Two of the abovementioned theories – (a) and (b) – explain the charge-generation phenomenon with the specific morphology and ionic structure of the ionic polymer membrane, while the role of the electrodes is of secondary matter. These theories apply on an ionic system, where one ionic species (SO_3^- anions in the case of Nafion as the ionic polymer membrane) is fixed to the polymeric backbone and the counter-ion (Li^+ , Na^+ , etc.) associates to the fixed ionic groups. The explanation (c) underlines the importance of the electrode material and predicts a stronger sensorial response from a laminate with higher specific surface area electrodes.

The charge-generation phenomenon is well characterized for the IPMCs with a single mobile ionic group. Simultaneously, ILs have been used as an alternative solvent and electrolyte for the IPMC sensors and actuators [55], while the use of IL is primarily motivated by its stable in-air operation capability. In the case of an ionic polymer membrane that is swollen in an IL, both cations and anions are the mobile ionic species. Mechanoelectrical transduction of the IPMCs with IL electrolyte has been investigated with the purpose of verification of the streaming potential hypothesis [51,56].

It has been underlined that some types of IEAP are capable of sensing also deformations other than bending, such as shear or compression [50,56]. Streaming potential or current, emerging in the electrodes, has been proposed as one of the underlying physical mechanisms for sensorial response in a wide range of configurations. The mechanism for the sensorial response is currently still under debate. However, it can be concluded that the choice of the most appropriate electrode material, as well as the choice of the membrane material, have both significant importance.

c. Conducting polymer-based IEAPs as motion sensors

In addition to the inert noble metal electrodes (such as platinum), also Faradaic conductive polymer [44,57–61] and (likewise Faradaic) ruthenium dioxide [51,56] electrodes have been suggested for construction of motion sensors. The earlier understanding of the formation of sensorial current was narrowing of the band gap of the conducting polymer due to stretching of the polymer backbone, in turn changing the density of states, and inducing redox current [57]. A more recent interpretation for the formation of the sensor signal involves *deformation-induced ion flux* – exerted mechanical strain induces a flux of mobile ions and causes a shift in the balance of ions between the polymer phase and the electrolyte [44]. Additionally, the change in the value of equivalent capacitance between the conductive polymer and electrolyte phase may also contribute to the sensor signal [61].

d. Carbonaceous IEAPs as motion sensors

The sensorial response of the IEAPs with carbonaceous electrodes has previously been reported only in few papers. Baughman *et al.* predicted in 1999, without experimental verification at that time, mechano-electrical effect in an IEAP with carbon nanotube electrodes [29]. Kamamichi *et al.* have fabricated carbon nanotube-based IEAPs, which yield ‘up to 0.1 mV’ sensor voltage in response to motion, by printing the electrode material on a cast PVdF-IL membrane [62]. Ghamsari *et al.* [63] have also mentioned, without experimental investigation, sensorial property of the IEAPs with bucky-gel electrodes. Otsuki *et al.* have constructed a bending speed-independent deformation sensor based on a non-specified solid polymer membrane and non-specified carbon electrodes, yielding output voltages of up to 350 mV [64]. *Per contra*, Akle *et al.* stated in 2012 that the IEAPs with high-surface-area (such as activated carbon- or carbon nanotube-based) electrodes ‘do not operate properly as sensors’ due to predictable complications in the signal-conditioning circuitry [56].

Carbon-based ionic sensors have also been constructed in other forms than laminates. Mirfakhrai, Baughman, *et al.* have used carbon nanotube yarns for measurement of tensile stresses [65]. However, this sensor works by measuring electric current between a biased yarn and a reference electrode. The sensorial effect is explained by an increase in the surface area of the yarns due to tensile force. Formally, this kind of sensor does not belong to the class of IEAP, also because no polymer is involved in its construction, but its supercapacitor-like structure suggests a similarity to IEAP in its working principle.

1.2.4 IEAP for sensing stimuli other than mechanical

There are only few attempts found in the literature on using the IEAP technology for measuring stimuli other than mechanical. In 2012, Bakhomou *et al.* proposed a miniature supercapacitor for measuring humidity level inside electronic component packages, or inside composite materials. The supercapacitor, constructed from activated carbon electrodes and having potassium hydroxide

electrolyte, was claimed to have the highest sensitivity with respect to its size among all known types of moisture sensors [66]. However, the proposed humidity-sensing mechanism proposed by Bakhoum *et al.* does not incorporate any generation of electric charge.

1.2.5 IEAP as an energy harvester

IEAP is characterized as a mechanoelectrical sensor in **Section 1.2.3**. As an IEAP is a passive type of sensor, *i.e.* it senses motion by formation of electric current, it is obvious that it could, in principle, be also used as an energy harvester unit to convert mechanical energy into electrical. From the viewpoint of IEAP composition, there is no fundamental difference between the sensors and the energy harvesters, as both devices are generally optimized for the largest mechanoelectrical effect.

From the class of IEAPs, energy harvesting capability from mechanical vibrations has been most widely explored in the case of IPMCs. An IPMC is applicable as a mechanoelectrical energy harvester in the frequency range of <50 Hz, has an efficiency of less than 2%, and generates instantaneous power of up to $45 \mu\text{W cm}^{-3}$ [67]. The IPMCs with water as a solvent are especially advantageous in underwater energy harvesting; that is, harvesting electric energy from water flow or vibrations [68–70]. This is due to the intrinsic water-compatibility of the IPMCs. Although the IL-based IEAPs (or IPMCs) are operable in air [71], in-air energy harvesting using these IEAPs has attracted incomparably lower level of interest. This can be due to the availability of more efficient alternative mechanoelectrical energy-harvesting materials – for example, polymer piezoelectrics yield roughly two times higher energy conversion efficiency, compared to the IPMCs [67]. For example, a solution for harvesting wind energy by fluttering motion of leaf-shaped cantilevers has been realized using polymer piezoelectrics [72].

1.3 Humidity-sensitivity of IEAP

A number of potential applications for IEAP, irrespective of the particular function of an IEAP in a device, require the ability for operation at a wide range of relative humidity (RH) levels. Ambient humidity is an important parameter that determines the performance of the IPMC actuators in air [73]. This is also expected, as its working mechanism is based on electro-osmosis of the water-solvated ions. In-air use of the IPMC motion sensors has been demonstrated; however, the sensing signal is severely dependent on the hydration level [74].

Space, which is one of the promising fields of use for IEAP [75], is an exceptional environment due to its inconsiderable ambient humidity content. The IEAPs with IL as an electrolyte have a stable performance even in high vacuum [76]; therefore, IEAP actuators, but presumably also IEAP motion sensors, are compatible to the space environment. On the contrary, a number of

other potential fields of application for IEAP actuators, such as compliant gripping and haptic feedback devices, presume reliable operation at the full range of RH levels. To date, IEAP energy storage elements are often characterized in an inert gas atmosphere, e.g. in a glovebox, which excludes any effect from the ambient humidity, but makes it difficult to predict the behavior of the IEAP in real-world applications. Encapsulation is one of the frequently proposed solutions to overcome the possible problems arising from the humidity-sensitivity, although, encapsulation does not provide long-term protection for the IEAPs undergoing high levels of strain [77,78].

In the existing papers, IEAP actuators and sensors are, as a rule, characterized in ambient air and at constant temperature, but the RH level is often not even specified. The knowledge on the behavior of the IL-based electrochemical systems, working in air at the full range of RH, is of crucial importance, irrespective of their field of application – actuation, sensing, energy storage, or energy harvesting. The effect of ambient humidity on the performance of the IEAP actuators or sensors with IL as the electrolyte is seldom discussed, as IL is considered being fully stable in ambient conditions. However, in a real electrochemical device working in air, IL cannot be considered as a solvent-free electrolyte. Recently, the investigation of physicochemical properties of the water-IL mixtures has attracted an extensive interest [79–82], primarily from the viewpoint of using the ILs as non-volatile solvents in chemical synthesis or in purification technologies. A change in the RH level also causes a drift in the electromechanical parameters of IEAP actuators and sensors. This, in turn, gives rise to the need for considering the RH level as an important input parameter for actuator control algorithms and as a correction parameter for sensors. Consequently, the characterization and modelling of the effect of RH level on the properties of IEAP is justified.

2. FROM SENSORS TO ENERGY HARVESTERS

Vibration, humidity, and pressure, which are common by-products of anthropogenic activity (such as thermal power stations or motor traffic) and accompany with various natural phenomena, offer virtually unlimited source for harvestable energy. The energy harvested from the surrounding environment is considered as *green* and *renewable*. Today, many of the ambient power sources are often not widely utilized, due to the lack of efficient energy-harvesting materials. Due to the high cost of the energy-harvesting materials and due to their comparably low power density, the energy harvested from the ambient environment is currently not considered as a potential replacement for nuclear or thermal energy. However, the energy harvesters in micro-scale are of particular interest for portable devices.

2.1 Energy harvesting in micro-scale

Energy harvesting in micro-scale (power consumption below one milliwatt per device) offers increasing interest especially due to the following issues:

1. It is expected that trillions of wireless sensor network (WSN) nodes with computational and memory capability are to be deployed in the environment around us and on our bodies in next five years' time [83]. Although the energy consumption per one device is small, the large number of devices leads to a significant total power consumption. Luckily, the state-of-the-art electronic components have become more energy-efficient. Microprocessors with a power consumption of only $7 \mu\text{W MHz}^{-1}$ have been developed for use in WSN nodes [84]. A large number of WSN nodes operate in a low-duty-cycle mode, which decreases the total power consumption even further [85]; therefore, even low-grade sources, previously considered as unprofitable or unavailable, can be used to harvest energy. The low power-consumption level of the WSN nodes suggests that the amount of energy required to power the WSN nodes could be drawn directly from the ambient environment [85].
2. There are a large number of different sources of energy in the environment; most of them are irregular in time. A more reliable and efficient energy harvesting can be achieved by collecting energy from all available sources, therefore increasing the total amount of harvested power and minimizing the time with no harvestable energy available.
3. Implantable (or wearable) medical electronic devices, which can be combined with lab-on-chip technology, are expected to be capable of autonomous operation during several years. The ability of harvesting energy *in vivo* is a considerable improvement in the field of medical electronics. Previously, Li *et al.* have demonstrated energy harvesting from the energy of a heartbeat using ZnO thin films [86].
4. In terms of cost per unit of power, the energy harvesting units are today, as a rule, not comparable to the conventional (thermal) power stations.

Instead, the advantages of the energy harvesters emerge in the small-scale power-generation units. For example, despite the the thermoelectric energy harvesting units have intrinsically low efficiency (<10 %), they retain this level of efficiency even down at the microwatt-level, where the conventional generators are already impractical [87].

2.2 The current role of supercapacitors in energy harvesting

In the state-of-the-art device set-ups that incorporate supercapacitors or IEAP actuators, it is prevalent that they are either actuated or charged using electric power, supplied from some external source. An IEAP actuator can be brought towards its initial position by consuming the stored charge by short-circuiting the electrodes, or by changing the polarity of the charging current. A supercapacitor is discharged in a similar fashion, yet the stored electric charge is consumed by some electronic device to perform useful work. Despite a large amount of electric energy stored in an IEAP actuator, this energy is, in the device prototypes constructed to date, not recycled and therefore wasted after every actuation cycle. This is partially due to the lack of appropriate electronics available for recycling of the energy. However, the capacitive actuator technology holds an essential advantage in front of, for example, actuators based on Joule heating – a large amount of the applied electric charge can, in principle, be recycled.

The supercapacitors are considered for use in energy harvesting applications essentially as the intermediary or, less often, as the main energy storage units [88]. The transient electric energy output of the energy-harvesting materials, especially in the case of piezoelectric materials, is of irregular nature. The high-voltage output spikes from a piezoelectric material are first rectified using semiconductor-based electronics, and the energy is consequently stored in a supercapacitor. After the terminal voltage of the supercapacitor has exceeded a threshold value, the harvested energy is available for consuming. The recent work by Sun *et al.* [89] is a representative example of the role of a supercapacitor in a piezoelectric energy harvesting system.

The transient output of the thermoelectric generators is changing slowly in time, compared to the irregular transient signal of the piezoelectrics, but their output voltage level is extremely low (in tens to hundreds of mV) and their internal resistance is in orders of magnitudes lower than that of piezoelectric crystals. In such case, an external charge-pumping unit is used to boost the voltage to a suitable level for charging a supercapacitor, which acts as an intermediary storage unit. The state-of-the-art, commercially available step-up converters, such as LTC3108 by *Linear Technology*, can boost voltages up from levels as low as 20 mV and therefore allow harvesting energy from thermal gradients as low as 1°C [90]; however, at a comparably low (<50%) efficiency.

2.3 Ambient humidity as an energy source

Water holds a significant amount of energetic potential, in addition to its employment in conventional hydroelectric generators. Salinity gradient between brine and fresh water has been considered as a power source already in 1979 [91]. More recently, supercapacitor-like structures with nanoporous carbon electrodes and ion-selective membranes have been employed for the same purpose [92]. Yet, this system requires full immersion in the liquids and pumping of water with different salinities consumes considerable amounts of energy as well. The maximum extractable energy by this method is only moderate – up to 192 Wh per cubic meter of mixed solution, even without taking the loss of energy in pumping into account [93]. Thus, operation in gas atmospheres would be much more desirable.

Ambient humidity is rarely considered as a source of electric energy in the engineering solutions. On the contrary, reversible sorption of ambient water by a non-homogeneous material is a common actuation mechanism in the nature. For example, a pinecone opens because of dehydration of a layered structure (*i.e.* a cone scale) with a non-homogeneous fiber orientation in different layers [94]. Therefore, ambient humidity holds a significant energetic potential.

It is well known that asymmetric and reversible absorption of water by hygroscopic materials can be used for producing mechanical work. In its simplest expression, this effect can be observed as curling of a sheet of paper due to moistening of one of its sides [95]. Recently, the research on soft biomimetic artificial structures using sorption of water for actuation has gained a rising interest, with a perspective of developing shape-morphing structures for soft robotics applications [96–98]. A straightforward solution for turning sorption effects in a hygroscopic PEDOT:PSS film into mechanical rotary or linear motion has been proposed by Okuzaki *et al.* [99,100].

The conversion of ambient humidity absorption energy into electric energy is a very novel approach – it was first demonstrated in the scientific literature in 2013, but it has already attracted a significant interest in the engineering community. Inspired by the natural phenomena, water vapor has been successfully employed in energy harvesting by Ma *et al.* in 2013 [101]. However, in the work by Ma *et al.*, humidity gradient was not converted directly into electric energy, but a fast and reversible, hydrolysis- and hydrogen-bonding-based actuation of a polypyrrole–polyol-borate polymer composite was converted to electric energy through incorporation of a layer of piezoelectric PVdF polymer [101]. Biological materials have also attracted attention as hygroelectrical energy harvesters. In 2014, Chen *et al.* have demonstrated a fast and reversible mechanical response of *Bacillus* spores to water gradients [102]. The cortex region of the *bacillus* spores undergoes strain as much as up to 50% as a result of hydration. The density of mechanical energy generated in the hydration process is extremely high – up to 60 MJ m^{-3} . In the hygrovoltic cell constructed by Chen *et al.*, the water sorption energy is first converted into mechanical

motion and subsequently transformed into electrical energy via an electromagnetic generator.

Electrokinetic energy harvesters, which use streaming current as a power source, are perspective for small-scale energy harvesting [103], because, in their simple implementation, they do not require any special engineered materials. A working electrokinetic device can be fabricated straightforwardly as an integral part of microfluidic devices. The efficiency of a streaming current-based energy harvesting system is significantly increased (up to 3% have been measured) in the case when the electric double-layers on the opposite walls of a microfluidic channel overlap, which can be achieved at channel heights below 75 nm [104]. However, fabrication of the microchannels with nanoscale dimensions by lithographic methods is complicated. For that reason, the use of microporous materials, such as materials having ion-selective, 50-nm nanopores, has been suggested [105]. All electrokinetic energy harvesters presume a pressure-driven water flow for operation. To date, only a very few solutions, which use sorption or diffusion effects for flow generation, have been presented. Borno *et al.* have investigated water evaporation-driven energy harvester, inspired by the water transport in trees [106].

3. RESEARCH MOTIVATION

As similar IEAP laminates are used for different applications, could IEAP also be turned into a multifunctional device? In the emerging field of soft robotics, a perspective field of application for the IEAP, multifunctional qualities are often required from its components. The fundamentally distinctive approach in soft robotics is the use of morphological computation – a soft robot is not composed of a large number of individual actuators and sensors. Instead, the whole robot's body is morphed, and the robot must be conscious of its current shape at all times [107]. The design principles employed in soft robotics are derived directly from the nature. The reliable gripping and grip releasing mechanism of the caterpillar legs, regardless of the shape and texture of the substrate the caterpillar is crawling on, is a perfect example of morphological computation in the nature [1]. From the perspective of developing new materials for soft robotics, the materials having concurrently the qualities of an actuator and sensor are sought. Today, the multifunctional properties of IEAP are currently only scarcely recognized [45,46,108]. This work focuses on the investigation of sensorial properties of the IEAP laminates that are concurrently operable as well as actuators and even energy storage units.

It is known from the prior art that the conjugated polymer laminates undergoing Faradaic reactions [46] and the ionic polymer-based laminates with fractal-grown metal electrodes (*i.e.* IPMC) [43,67] respond to external mechanical stimuli by formation or variation of voltage and current between their electrodes. However, the working principle of the IPMC motion sensors is to date explained by more than one competing theory, as it is explained in **Section 1.2.3**. The previous research has been focused on modelling of the motion of ions and solvent in the ionic polymer cluster network. On the contrary, the significance of the surface area, porosity, and porosity distribution of the electrode material on the sensorial response has not been thoroughly investigated before. The aim of this thesis is to fill this gap.

This research is focused on the investigation of charge-generation properties of the IEAP laminates with non-Faradaic, high-surface-area activated carbon electrodes. In particular, the IEAP laminates with carbons derived from metal carbides – that is, CDCs – as the active electrode materials are investigated. This is due to the high specific surface area and the tailored porosity distribution of the CDCs.

Sensorial response is investigated on the IEAP laminates with and without ionic polymer as the membrane and polymeric binder. Hydrophilic IL is selected as an electrolyte for all of the investigated IEAP laminates.

At first, activated carbon-based IEAP laminates are considered as motion sensors, capable of determining the magnitude of an externally imposed curvature change. The mechano-electrical measurements involve characterization of the IEAP's response to different curvature change magnitudes, and characterization of the frequency-response of the IEAP motion sensors.

IEAP technology has, to date, only occasionally used to sense stimuli other than mechanical, as it is underlined in **Sections 1.2.4** and **1.2.5**. The high hygroscopicity of IEAP, covered in **Section 1.3**, suggests that IEAP laminates could have an electrically measurable response also in response to the level of ambient humidity. Therefore, a hypothesis is proposed that the sorption of ambient water vapor by an IEAP laminate can result in generation of a macroscopic electric charge. The humidity-sensitivity of IEAP would considerably broaden its field of application towards new types of differential sensors. In addition, the knowledge on the humidity-sensitivity of IEAP also gives valuable information on the behavior of IEAP as an actuator and as an in-air-operable flexible supercapacitor. The charge-generation mechanism is expected to be similar in either case – mechano-electrical or hygro-electrical transduction.

An IEAP laminate is a passive sensor that produces electric current and voltage in response to external stimuli. This suggests its outlook also as an energy harvester. A humidity-responsive IEAP would find use in humidity sensing and even micro-scale energy harvesting. In this work, for the first time, ambient humidity gradient is converted directly, without intermediary conversion into mechanical energy, into electric energy. Additionally, for the first time, storage of harvested electric energy into the same energy-harvesting material is demonstrated.

This work is organized as follows. **Section 4** generalizes the IEAP's charge-generation property from various external stimuli: in addition to mechanical stress, also ambient humidity is considered as an input stimulus. The design considerations for IEAP sensors are discussed in **Section 4.2** and the choice of materials for IEAP construction is discussed in **Section 4.3**.

Manufacturing of IEAP is not in the scope of this work; two different existing types of IEAP laminates were selected for the investigation of sensorial properties. **Section 4.4** gives the main characteristics for the chosen particular IEAP laminates.

The motion-sensing properties of the investigated IEAP laminates with carbide-derived carbon electrodes are investigated experimentally in **Sections 5.1-5.3**. The results are given in **Sections 5.4-5.5**.

Before the investigation of humidity-induced charge-generation properties, it is necessary to characterize the changes in the electrical properties of IEAP under different RH levels. This is done in **Section 6**. Humidity-sensitivity of IEAP is investigated experimentally in **Sections 6.2-6.3**. An equivalent circuit for IEAP is proposed in **Section 6.4** and the changes in the equivalent circuit parameters, as a result of humidity absorption, are analyzed by impedance spectroscopy in **Section 6.5**.

IEAP's response to a humidity gradient is investigated experimentally in **Section 7**. The revealed extensive response of an IEAP to ambient humidity gradient suggested that the IEAP could be employed even in energy harvesting. **Section 8** characterizes IEAP as a hygro-electrical energy harvester.

4. SENSORIAL PROPERTIES OF IEAP

4.1 Working principle

This work investigates IEAP as a sensor for detecting either motion or ambient humidity. As explained in **Sections 1.2.3** and **1.3**, an IEAP can be used in a variety of configurations to sense motion or humidity. This work explores IEAP sensors in one specific configuration – a transducer converting bending motion (**Section 5**) or humidity absorption (**Section 7**) directly into electric current and voltage. Conversion of both stimuli into an electrical signal is explained, in this thesis, by a similar underlying physical process; therefore, the underlying mechanism is provided jointly in this section.

Voltage or electric current could not be registered between the IEAP electrodes if completely symmetrical physical processes take place in both of the opposing electrodes. Nevertheless, charge-generation by applying equal mechanical strain on both electrodes of an apparently symmetrical IEAP has been reported in the literature [50,56]. For generation of electric current and voltage as a response to various stimuli, IEAPs could be engaged in at least two configurations – (a) an asymmetric IEAP laminate being exposed to homogeneous stimuli, or (b) a symmetrical IEAP laminate being exposed to non-homogeneous stimuli. The current work is concerned on the latter approach: electric charge is generated as a result of mechanical strain or humidity gradient applied across a virtually symmetrical IEAP laminate.

The carbonaceous electrodes of the IEAPs used in this work are assumed to be ideally polarizable, *i.e.* there is no charge transfer across the electrode-electrolyte interface. Whenever an electrode is brought into contact with an electrolyte, two accompanying phenomena occur: (a) reorientation of electrolyte ions, which can also cause reorientation of solvent molecules; and (b) redistribution of electrons in the electrode surface for balancing of the total charge [109]. As a result, the charges accumulate on the boundary, forming a so-called electrical double-layer.

It is important to identify the difference between charging of an IEAP externally, using an external power source, and internally, which occurs in the case of an IEAP employed as a sensor. When an IEAP is used as a supercapacitor or an actuator, electrons are injected to or drawn away from its electrodes. The charge is balanced in the electric double-layer region by reorientation and dislocation of the electrolyte ions, as illustrated in Figure 1A – the electrode that has negative electric potential attracts cations. An IEAP, operating as a sensor, is illustrated in Figure 1B. If an IEAP is used as a sensor, the electrolyte ions are dislocated and reoriented due to some adventitious phenomena. The originally symmetrical electric double-layers at the opposite electrodes undergo unsymmetrical processes, and they are rearranged in an unequal fashion. Therefore, the difference in the charge distribution is also induced in the electrodes.

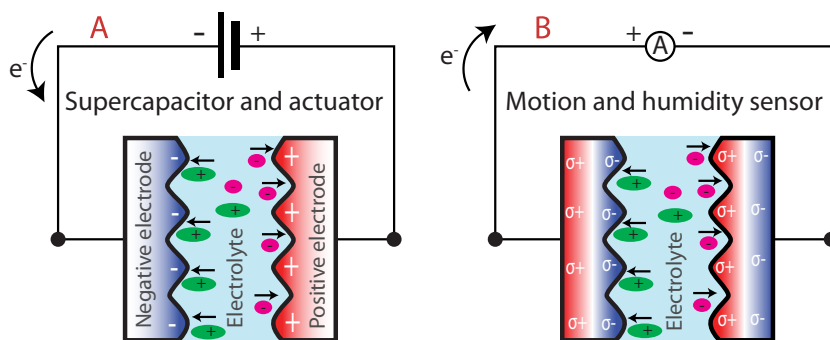


Figure 1. Motion of the electrolyte ions in the electrolyte, redistribution of electric charge in the electrodes, and the corresponding polarity of electric potential between the electrodes when an IEAP is charged (A) using an external current source in the case of supercapacitors and actuators; or (B) by directional motion of the electrolyte ions in the case of motion or humidity sensor.

A shift in the charge distribution in at least one electrode induces electric current across an external electric circuit that is connected between the electrodes (Figure 1B). An external workload and a current-measurement resistor are examples of external electric circuits. If the generated electric charge is not consumed by an external circuit, the total number of electrons in either electrode is not changed, and the charge balance is achieved by shifting the electron density within a single electrode. The electrode with an excess of cations in its electric double layer region balances the total charge by involving more electrons; a measurement circuitry connected between the opposite electrodes indicates this electrode as having positive potential (Figure 1B).

4.1.1 Mechanoelectrical transduction

Externally induced bending of an IEAP laminate causes compressive stress in the electrode at the concave side and tensile stress in the electrode at the convex side of the IEAP. Consequently, dissimilar conditions for the opposite electrodes are straightforwardly achieved. The bending motion induces an unidirectional pressure-driven flux of electrolyte within the microporous electrode and within the polymer matrix, swollen by the electrolyte. Formation of electric current or potential between the electrodes can be achieved, when the mobilities of the differently charged ions in the given porous structure are dissimilar. Different cation and anion mobilities can be induced by (a) appropriately matching the porosity distribution of the electrode material with the sizes of the ions of the particular electrolyte; or (b) by tailoring the interaction between the electrolyte ions and the polymer matrix. In this work, the mechanoelectrical effect was enhanced by the use of the carbonaceous electrode materials with appropriately chosen specific porosity distribution. This, in turn, results in unequal mobilities of the electrolyte ions that have different lateral dimensions.

4.1.2 Hygroelectrical transduction

As a hypothesis, reorientation and/or dislocation of the mobile ions could also be achieved merely by hydration of the hygroscopic constituents of the laminate. The hygroscopic ions can collect water molecules into their solvation shell; therefore, their effective volume increases. The change in the effective volume of ions can alter the structure of electric double-layer at the electrode-electrolyte interface. Therefore, the high hygroscopicity of the constituents of IEAP is the primary concern in its employment as a hygroelectrical transducer.

A hygroelectrical transducer requires a particular match between the porosity distribution of the electrode material and the electrolyte. Therefore, the optimization criteria for the design of hygroelectrical transducers are in a good agreement with the criteria for the design of mechanoelectrical transducers. Consequently, it is expected that an IEAP that has strong mechanoelectrical response and consists of hygroscopic materials also performs well as a hygroelectrical transducer.

An important qualitative difference between the hygroelectrical and mechanoelectrical transduction is the possibility for long-term conservation of perturbations in the double-layer in the case of hygroelectrical transducers. It is obvious that an IEAP laminate can be bent only up to its finite maximum curvature (numerically equal to the reciprocal of the laminate's thickness); therefore, the maximum amount of generated charge in one bending cycle is strictly limited. After a sufficient time of waiting, the perturbations in the double-layer are leveled off and the bent position then corresponds to a newly achieved stable state. In contrast, an uniform humidity gradient can be maintained across an IEAP during a virtually unlimited time. Long-term conservation of a humidity gradient can give rise to continuous diffusion of water and water-solvated ions in the IEAP's thickness direction. Consequently, a considerably higher amount of electric charge per one cycle can be generated by applying humidity gradient rather than strain gradient between the IEAP's electrodes.

4.2 Considerations for design of IEAP sensors

In the selection of materials for an IEAP working solely as a supercapacitor, it is beyond doubt that the surface of the carbonaceous electrode material must be easily accessible for both anions and cations [40]. For an IEAP intended to be employed as an actuator, it is generally accepted that higher ionic conductivity of the electrolyte-containing polymeric membrane increases the actuator's response speed, while the generated strain depends (a) on the interaction between the ionic moieties and (b) the specific surface area of the electrodes, which, in turn, determines the amount of transported charge [8,110-114]. The actuation property is related to the different sizes of the oppositely-charged ions [113].

As a hypothesis, the sensorial response of an IEAP can be enhanced by selecting such combination of IL and porous matrix, where the mobilities of

cations and anions are purposely dissimilar. Unequal mobilities can be achieved by (a) tailoring the relation between the porosity distribution of the microporous electrode and the sizes of the IL ions; (b) tailoring the interaction between the electrolyte ions and the ionic polymer membrane; and (c) by selective hydration of the hydrophilic ionic groups. These optimization criteria are expected to slow down the charge-transfer kinetics of an IEAP significantly, therefore making it less favorable to be used as an energy storage unit.

It is demonstrated in this thesis that an IEAP with eminent actuation capability operates equally well as a sensor. Therefore, the investigation of sensorial response of IEAP may lead to a conclusion that unequal mobilities of the electrolyte ions in an IEAP can result in a higher strain-generation capability. As it is underlined in **Sections 1.2.2** and **1.2.3b**, the actuation and sensing mechanism can be easily explained in a system with anions permanently fixed to the ionic polymer backbone. In the IEAP laminates used in this work, both ionic and non-ionic polymers are used as a separator and binder. This enables to identify the role of the electrodes on the sensorial response of the carbonaceous IEAP. It is expected that the porosity distribution of the activated carbon-based electrodes has a strong influence on the laminate's sensorial properties. Therefore, special attention is paid on the choice of electrode material and the congruence between the electrode material and the electrolyte.

4.3 Selection of materials

In this work, the IEAP laminates with activated carbon (in particular, CDC) electrodes, IL electrolyte, and different polymeric separators are considered. The selection of the particular materials for IEAP is explained as follows.

4.3.1 CDC as an electrode material

CDC is obtained by chlorination of metal carbide (SiC, TiC, B₄C, Mo₂C, VC, etc.) precursors at high temperature (400–1200°C) in an oxygen-free atmosphere [7,115,116]. During the chlorination process, the metal atoms are selectively extracted from the crystalline precursors, preserving the precursor's original structure, shape and volume. The properties of the CDCs are highly dependent on the chlorination temperature and the choice of precursor, as the distribution of carbon atoms in the carbide precursor lattice is different. Furthermore, CDC is subject to post-synthesis annealing, typically with H₂ or NH₃, which is necessary for the removal of chloride residues, but the surface area and structure of CDC can also be affected during the annealing process [117]. The unique possibility of tuning the porosity in sub-angstrom accuracy in the nanometer-range, its high specific surface area (1000-2000 m² g⁻¹), and its chemical inertness make CDC attractive for use as supercapacitor or lithium battery electrodes [118], in capacitive desalination [119], and even as gas storage medium [120]. CDC is formed on the surface of the precursors and it is

therefore possible to control the thickness of the resulting CDC layer; however, structural variations can arise in its thickness direction [121]. In fact, CDC can contain a variety of different carbon nanostructures from planar graphite to carbon nanotubes, onion-like structures, and nanodiamonds [122]. The composition of a particular CDC is dependent on its synthesis parameters.

Bulk CDC is usually produced from carbides that are in the form of fine powder; therefore, the resulting CDC is also a fine-grained powder by its consistency. As a rule, IEAP electrodes are fabricated from a CDC powder that has been fully chlorinated, *i.e.* it is supposed not to contain its precursors – metal carbides. It has been demonstrated that CDC, unlike the majority of activated carbons, is fabricable by lithographic methods [123,124]. This makes CDC distinctive in the field of high-surface area carbons, as it opens a possibility to produce electrochemical devices with CDC electrodes in micro- or nanoscale.

CDCs can be considered as hydrophilic materials. The CDC synthesis produces a carbon material with a low amount of carboxyl, carbonyl, or hydroxyl functional groups [116]. However, upon the first exposure to air or in the process of post-activation, the dangling carbon bonds formed in the synthesis procedure are quickly functionalized [125]. This determines the hydrophilicity of CDC.

As also mentioned in **Section 1.2.3d**, the motion-sensing properties of the IEAPs with carbonaceous electrodes have not been comprehensively characterized previously. The advantages of CDC compared to other types of activated carbons, listed in the paragraph above, motivate the selection of CDC as an electrode material for IEAP sensors. Two different CDCs, derived from boron carbide (with rhombohedral crystal structure) or titanium carbide (with cubic crystal structure), were considered in this work. The corresponding CDC is referred to as B₄C-CDC or TiC-CDC, accordingly to the precursor for the CDC synthesis. This nomenclature has been suggested by Presser *et al.* [7]. B₄C-CDC is produced by Y-Carbon Inc. and TiC-CDC by Skeleton Technologies. The porosity distributions of the CDCs, given in Figure 2, were measured in the Institute of Chemistry, University of Tartu. Nitrogen adsorption method at the boiling temperature of nitrogen was used. The size distribution of pores below 2 nm is rather similar between B₄C-CDC and TiC-CDC, with the exception of a more pronounced peak at 0.54 nm in the case of TiC-CDC. The peak located at 0.54-nm pore size is clearly distinguished in the case of both CDCs. The pore distribution of B₄C-CDC is considerably wider – the amount of pores in the range of 2–8 nm is demonstrably higher than in the case of TiC-CDC. A wider porosity distribution can be advantageous, as it enables faster ion transport between the bulk electrolyte and the smaller range of micropores. It has been experimentally confirmed on ethyl-3-methylimidazolium bis-((trifluoromethyl)sulfonyl)imide (EMITFSI) IL that both anions and cations of the IL enter and exit the pores of TiC-CDC during charging and discharging [126].

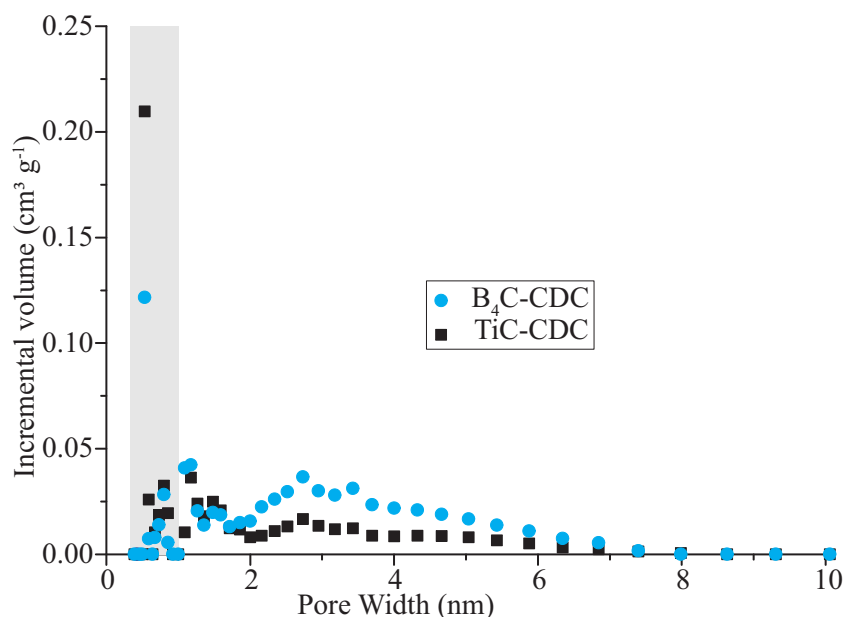


Figure 2. The porosity distributions of the CDCs used in this work.

4.3.2 IL as an electrolyte

Negligible vapor pressure has attracted IL to be used as a favorable electrolyte for the electrochemical devices that are operated in air [127]. ILs are often classified as hydrophilic or hydrophobic [80]. In this work, the IEAPs containing two hydrophilic ILs – EMITFS and EMIBF₄ – are considered.

In the case of majority of the ILs currently available, the cations are larger than the anions. The ILs used in this study – EMIBF₄ and EMITFS – also follow this trend. Both of the ILs have 1-ethyl-3-methylimidazolium cations, which are slightly oblong-shaped with lateral Van der Waals dimensions between 0.53–0.95 nm, based on quantum chemical calculations. The Van der Waals dimensions of spherical tetrafluoroborate and almost spherical trifluoromethanesulfonate anions are 0.47 and 0.58 nm, respectively. Therefore, by comparing the effective sizes of the ions with the porosity distribution of the CDC in Figure 3, it can be expected that the mobility of cations and anions of these ILs is unequal in the CDC porous network.

Water sorption changes almost all physicochemical parameters of ILs. As a rule of thumb, water content increases its conductivity (up to a water content level of 3-10 moles of water per a mole of IL [128]) and decreases its viscosity [82,128-130]. The high affinity towards sorption of vapors and a low vapor pressure enables the use of ILs as active elements in amperometric [131] or quartz crystal microbalance-based [132] sensors.

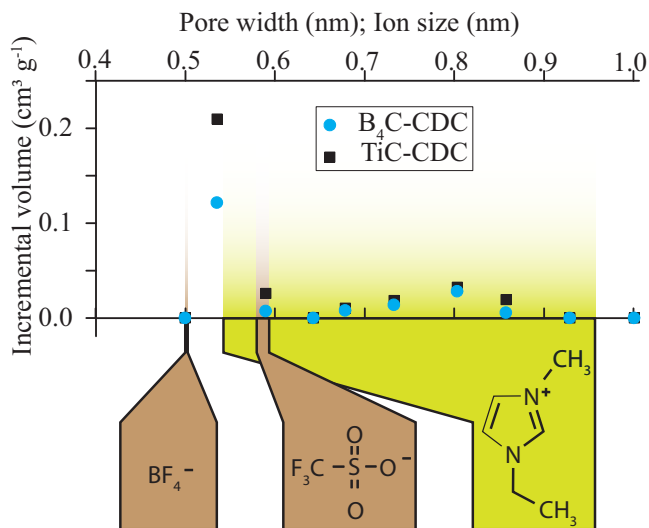


Figure 3. Comparison between the lateral sizes of the IL ions used in this work and the porosity distribution of the CDCs.

Although pure ILs consist entirely of ions, it is not correct to assume that all the ions contribute to its electric conductivity. For a reference, the effective ionic concentration of pure BMIBF₄ and BMITFS ILs are only 0.64 and 0.57, respectively, of their respective molar concentrations [133]. Therefore, a pure IL could be considered as a system, where some of the IL ion pairs act merely as a solvent. What is more, in a real electrochemical system operating in air, the absorbed water acts as an additional solvent [128]. Increase in the molar fraction of water in the IL-water mixture increases its conductivity, in part due to increase in the effective ion concentration. Table 1 compares the conductivities of the ILs used in this work in their pure form and in mixture with water. It is seen that the IL:water molar concentration corresponding to the highest conductivity is below 0.2, and the conductivity of an IL:water mixture can be as much as 6 times higher than that of corresponding pure IL.

The hydrophilicity of ILs is determined, as a rule, by its anions, especially if the anions have a high charge-per-volume ratio [82]. The TFS⁻ anion is highly hydrophilic due to its sulfonate group. The imidazolium-based cations are considered hydrophobic; thereby, the hydrophobicity increases with the length of its hydrocarbon chains. Therefore, the EMI⁺ cation is the least hydrophobic cation from the group of imidazolium-based cations [79]. In addition, the positive charge on the EMI⁺ cation is specifically located on the imidazolium ring, which makes the total charge distribution over the EMI⁺ cation anisotropic and causes its specific orientation on adsorption [137]. Therefore, it can be assumed that (a) also the EMI⁺ cations can also bind water molecules; and (b) the equilibrium orientation of the EMI⁺ cations can be different at various sorption degrees.

Table 1. Conductivities of IL-water mixtures

	EMIBF ₄	EMITFS
Conductivity in pure (water-free) form, S m ⁻¹ at 298 K	1.55 [134]	0.98 [135]
IL:water molar fraction corresponding to the highest conductivity	0.12 [134]	Below 0.2 [136], exact value is not found in the available literature
Highest conductivity in mixture with water, S m ⁻¹ at 298 K	9.2 [134]	3.93 (at IL:water molar fraction of 0.2) [136]

4.3.3 Polymeric separator and binder

The IL-incorporated polymeric membrane has a strong influence on the performance of IEAP, as the morphology and ionic moieties in the polymer determine its ion-transport characteristics [3,8,138].

Extensive swelling of ionic polymers in hydrophilic ILs [71] and the resulting higher ionic conductivity [139] has led to a wide use of the IL-integrated ionic polymer electrolytes as membranes in various electrochemical devices [6,140]. Nafion – a polymer with tetrafluoroethylene backbone with random inclusions of perfluorovinyl ether groups terminated with sulfonate groups – is widely employed as separator material for IEAP actuators and sensors.

The anionic sulfonic acid groups are highly hydrophilic – Nafion can absorb as much as 22 wt% of water [141]. Each sulfonate group in Nafion can coordinate up to 23 water molecules [142]. The hydration of Nafion changes both its physical and electrical properties. The performance of the IPMC actuators in air is directly related to the water desorption kinetics [77] – dehydration of Nafion decreases the performance of IPMCs at low RH due to a decrease in the ionic mobility. In turn, an IPMC-like electrochemical system has been applied as a humidity sensor, where the ambient relative humidity value is extracted by measuring electrical impedance between the electrodes [143]. There exist also other approaches for applying Nafion for sensing humidity – *e.g.* measuring its weight change by the use of quartz crystal microbalance method [144].

Nafion also swells extensively in hydrophilic ILs – it can absorb EMITFS as much as 60% of the dry weight of the membrane [145]. Incorporation of a large amount of water or hydrophilic IL creates a cluster channel network into Nafion, thus providing a path for the mobile ions to be dislocated. A Nafion network, highly swollen in an IL, contains and conducts both cations and anions [146]. As illustrated in Figure 4A, the cluster network in Nafion that is swollen only in EMITFS consists of EMI⁺ cations that are bound with the sulfonic acid groups of Nafion, and free IL that is acting as a solvent. The addition of water (Figure 4B) causes hydration of strongly hydrophilic functional groups – the sulfonic acid groups in Nafion, and the TFS⁻ anions. Consequently, the IL ions become more mobile in the cluster channels in Nafion. The diffusion coefficient for the cations and anions of an IL in a hydrated ionic polymer matrix is a

complex topic – it has been demonstrated that the conductivity of cations is higher in low water content due to formation of triple-ion complexes with two anions and one cation. Instead, the mobility of cations is constrained by their interactions with the ionic moieties of ionic polymer at high water content [146].

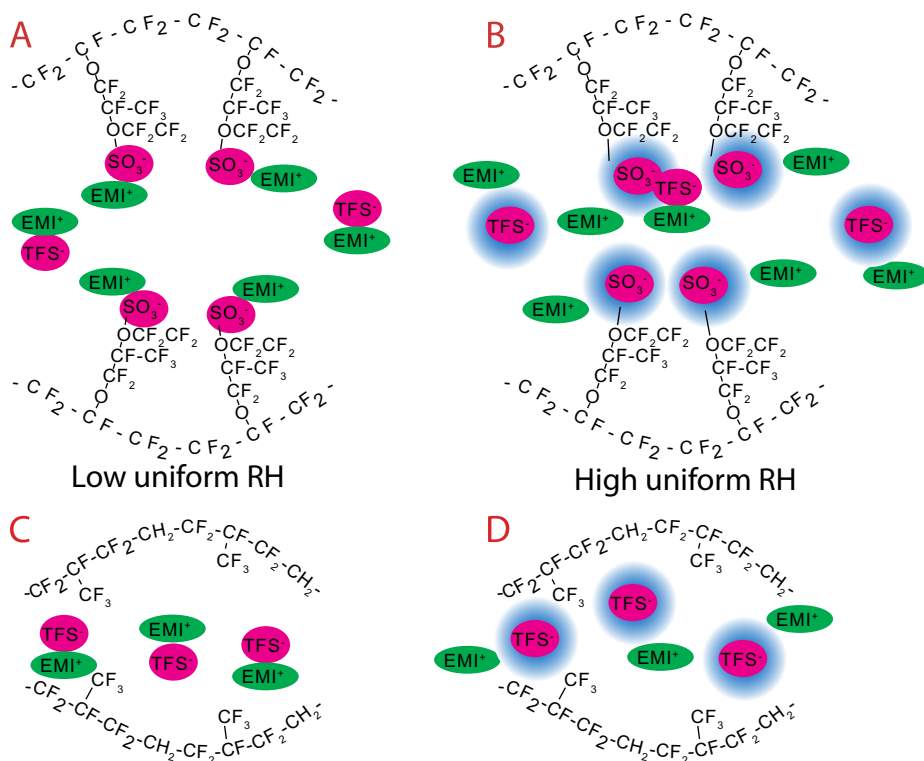


Figure 4. Cluster network in Nafion incorporated with IL (A) in dry and (B) in hydrated state. IL-incorporated PVdF-HFP polymer (C) in dry and (D) in hydrated state.

The choice of polymers is not limited with ionic polymers – ILs have been successfully incorporated into non-ionic polymers such as PVdF-HFP (Figure 4C) [32,33,38]. The PVdF-HFP matrix is hydrophobic; therefore, the change in the RH level can influence the mobility of ions in the PVdF-HFP matrix only as a result of hydration of the ions themselves (Figure 4D).

A more recent approach in the development of polymer electrolytes for IEAP is the synthesis of self-assembled, nanostructured, sulfonated block copolymers with well-connected ionic channels, which allow fast and organized motion of IL [8]. Another approach in obtaining solid (structural) electrolytes, suitable for IEAP, is the synthesis of polymerized ILs [147].

4.4 The IEAP laminates investigated in this work

In this work, two different types of IEAPs with tailored properties were chosen for the investigation of mechanoelectrical and hygroelectrical properties. These IEAPs, referred to as Type I and Type II, differ from each other in the selection of materials and the manufacturing method.

IEAP Type I is prepared using *direct assembly process*. This process was first used to fabricate IEAPs by Akle *et al.* in 2007 [148] and it was further developed by Palmre *et al.* [149]. This type of laminate has a good performance as an actuator – it undergoes peak-to-peak strain of 2.3% at 2 V input signal, and a 8-mm-wide strip can exert 3.6 mN blocking force at a distance of 40 mm from its fixing point [149].

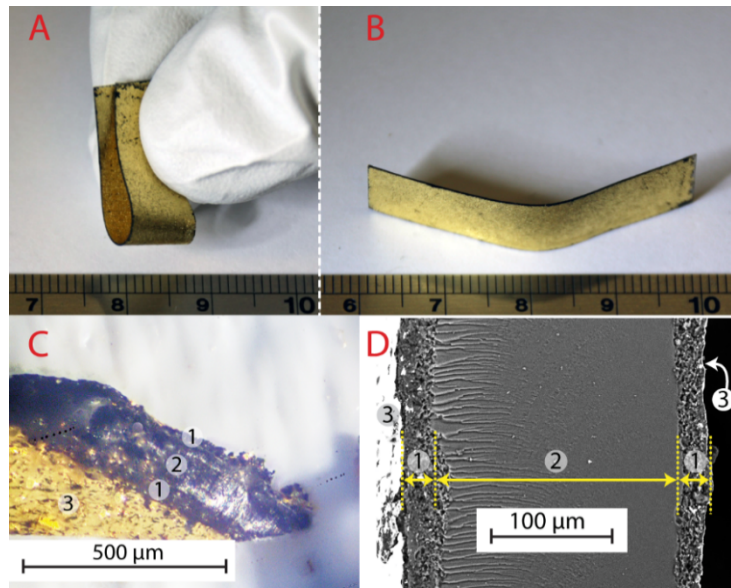


Figure 5. (A) Flexibility of the IEAP laminate Type I. (B) Residual deformation of the IEAP after bending. (C) Optical micrograph of an IEAP Type I cut slantwise. (D) Scanning electron micrograph of the cross-section of an IEAP Type I. (1: electrode; 2: membrane; 3: gold current collector.)

The finished laminate is highly flexible – it can be easily bent to radii below 3 mm without delamination, cracking of the electrodes, or discontinuation of the gold current collector, as shown in Figure 5A. The material is, however, slightly viscous – the neutral position shifts after bending it to high curvatures, as seen in Figure 5B. The cross-section of the prepared IEAP is shown using an optical microscope in Figure 5C and using a scanning electron microscope in Figure 5D.

IEAP Type II is prepared by layer-by-layer casting. This method was developed for fabrication of IEAPs by Fukushima *et al.* in 2005 [32] and it was further developed by Torop *et al.* [38,150]. This type of IEAP functions as an actuator – an actuator, 7 mm in width, can exert 79 mN force at 2.8 V [150]. However, its time response is considerably slower than in the case of IEAP Type I.

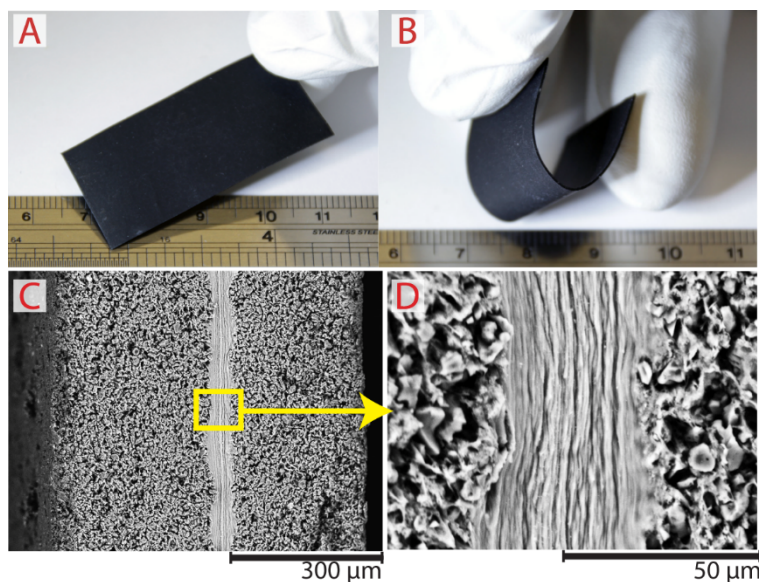


Figure 6. Photographs of an IEAP Type II in (A) straight and (b) bent state. Scanning electron micrographs of (C) the cross-section of the IEAP; (D) the electrode-membrane interface. C-D are adapted from [151].

The finished laminate is highly flexible, as shown in Figure 6A and B. Scanning electron micrograph given in Figure 6C shows that the finished laminate has 220-μm electrodes and a 30-μm membrane. Figure 6D gives a close-up to the electrode-membrane interface.

The main characteristics, relevant to this work, of IEAP types I and II are compared in Table 2.

This work considers the IEAP's response to motion and RH. Long-term use of EMIBF₄ is not recommended, however, for applications that require operation in high-humidity conditions due to hydrolysis of BF₄ ions [152]. Therefore, only the IEAP with EMITFS, one of the most hydrophilic ILs, as the electrolyte (that is, IEAP Type I) is selected for the investigation of humidity-related effects in this work. Table 3 summarizes the use of different types of IEAPs in the experiments conducted in this work.

Table 2. The comparison between the laminates Type I and II.

Characteristic	IEAP Type I	IEAP Type II
Electrode material	TiC-CDC	B ₄ C-CDC
Separator and binder polymer	Nafion	PVdF-HFP
Electrolyte	EMITFS	EMIBF ₄
Manufacturing method	<i>Direct assembly process</i>	Layer-by-layer casting and hot-pressing
Current collector	~130-nm Au	–
Electrode thickness (each)	30 μm	220 μm
Separator layer thickness	190 μm	30 μm
Relative thickness of the electrodes to the total thickness	24%	94%
Carbon:polymer ratio in the electrodes, wt%	41:59	68:32
Electrode resistance	<1 Ω square ⁻¹ (with current collector)	28 Ω square ⁻¹
Cross-electrode impedance module at 1 Hz	28 Ω cm ² (at 53% RH)	66 Ω cm ²

Table 3. The use of different types of IEAPs in this work.

Stimulus	Sensorial properties	Energy harvesting
Motion	IEAP Type I and II	IEAP Type I and II
Humidity	IEAP Type I	IEAP Type I

5. IEAP AS A MOTION SENSOR

5.1 Characterization of IEAP motion sensors by homogeneous bending

The motion-sensing properties of IEAP are, by default, measured in a cantilever configuration, because it also corresponds to their usage and measurement configuration in actuation mode. In this way, a multifunctional device simultaneously having sensorial and actuation capability is achieved.

An unloaded, cantilevered actuator can bend homogeneously, if it has inconsiderable voltage drop along its electrodes. The electronic conductivity of the electrodes can be enhanced by using current collectors on top of the electrodes. In this work, IEAP Type I, which has current collectors made of gold, stands out for its low surface resistance of $<1 \Omega \text{ square}^{-1}$. Therefore, the free part (the part which can freely bend without obstructions, *i.e.* it is not clamped between the electric terminals) of the IEAP actuator always has a homogeneous curvature.

Characterization of the sensorial properties of IEAPs is more complicated, as it is difficult to bend the IEAP homogeneously and continuously in time. Homogeneous bending of an IEAP motion sensor is advisable for two reasons:

1) When an IEAP is bent homogeneously, the measured data represents essentially the material properties, not the peculiarities of a particular device configuration. The mechanoelectrical parameters measured by homogeneous bending can be afterwards used to predict the output of sensors in other, non-homogeneous bending configurations.

2) This configuration corresponds to the use of IEAP motion sensors in potential applications; *e.g.* by coupling the motion-sensing IEAP to an IEAP acting as an actuator. In this way, the IEAP operating as a sensor can give feedback corresponding to the actuation speed and magnitude to a controller that drives the IEAP operating as an actuator [153,154].

From a contrasting point of view, there are also a number of perspective biomimetic applications for the IEAP sensors in non-homogeneous bending configurations – *e.g.* hair flow sensors [155,156] or tactile sensors [154]. Airflow has also been previously used to induce actuation in characterization of IPMC sensors [157].

A large number of scientific papers describe characterization of IEAP motion sensors by applying external force on the free end of the cantilevered actuator in a direction that is perpendicular to the initial (unbent) position of the IEAP [44,53,60,74,158-160]. In this way, the material under investigation can be bent in a virtually unlimited frequency range, but the maximum achievable bending deflection is limited. Biddiss *et al.* [161] have used a measurement configuration, where one end of the cantilever was fixed to a rotating platform. By doing so, the deflection amplitude is increased at the cost of decreased frequency range. In addition, the bending curvature is still nonhomogeneous at high bending angles.

To date, several techniques have been developed for measurement of bending motion sensors at constant curvatures. The most straightforward solution is fitting an IEAP sheet to surfaces of cylindrical objects with different diameters [162,163], or sliding an IEAP on the surface of a test block between sections with different curvatures [64]. However, continuous and smooth change in the curvature could not be achieved using these two methods.

5.1.1 Rigs for homogeneous bending of the IEAP

To overcome the limitations imposed by the previously existing measurement methods, two custom-made, previously unexampled bending rigs were constructed in this work. They are referred to as Test rig A and Test rig B in this thesis. These bending rigs are characterized by the capability of bending IEAP motion sensors to large curvatures at high speed, while maintaining homogeneous bending curvature of the sensors at all times. The main parameters of the bending rigs are compared in Table 4. The construction and working principles of the rigs A and B are given in detail in papers I and II, respectively.

The usable frequency range for some types of IEAP motion sensors can reach over 33 Hz [164], yet at very small deformations. In this work, the IEAP's ability of measuring extremely high bending deflections (up to $\pm 121 \text{ m}^{-1}$) at moderate frequency range (up to 3 Hz) is investigated. Such conditions correspond to the IEAPs applied in haptic feedback systems or as feedback sensors for the same material acting as an actuator. Additionally, there exist a variety of other actuator and sensor technologies (*e.g.* piezoelectric actuators and sensors) for generation and measurement of small strains ($\ll 1\%$) at high frequencies ($> 100 \text{ Hz}$), but the capability for achievement and measurement of very high deformations ($> 1\%$) is one of the distinctive characteristics of IEAP.

Table 4. Parameters for the bending rigs used to investigate motion-sensing properties of IEAP.

	Test rig A	Test rig B
Homogeneous bending profile	Yes	Yes
Smooth change of curvature in time	Yes	Yes
Sinusoidal transient curvature	(not implemented)	Yes
Bending speed	Full bending cycle in $< 5 \text{ s}$	3 Hz
Achievable curvatures	20- 60 m^{-1}	$\pm 121 \text{ m}^{-1}$

5.2 Transient response of IEAP Type II

5.2.1 Experimental set-up

The transient response of IEAP Type II motion sensor to steep bending was characterized using Test rig A, which allows achievement of bending curvatures in the range of 20–60 m^{-1} .

The experiments were performed in the following order:

1. holding the laminate in still position at a curvature of 20 m^{-1} (radius r_0 in Figure 7 A) for at least 500 s for achievement of equilibrium conditions;
2. steep bending of the laminate to a different curvature (radii r_1 – r_3 in Figure 7A);
3. holding the laminate at its newly-achieved curvature for 500 s;
4. returning the laminate steeply to its initial curvature;
5. holding the laminate in still position for another 500 s.

During the whole experiment, electric current or voltage was registered. Open-circuit voltage was measured by connecting the measurement terminals to a National Instruments' PCI-6036E analog input data acquisition (DAQ) device with an SCC-AI06 analog input module. Electric current was measured as a voltage drop over a 5- Ω resistor connected between the measurement terminals. The same DAQ set-up was used for the measurement of open-circuit voltage and electric current. Separate experiment sets were conducted for measurement of voltage and electric current.

5.2.2 Results

Transient course of open-circuit voltage, depicted in Figure 7F, and short-circuit current, depicted on Figure 7G, were both characterized by formation of a sharp peak immediately after steep bending (the transient bending profile is given in Figure 7E) and by slow diminishing of the signal to zero in 100 s. The electrode that was stretched out during bending obtained positive potential with respect to the electrode that was compressed. After 100 s, the course of voltage with opposite polarity was registered. The sign of the potential, however, switched always at approximately 100 s after bending, independent of the bending amplitude. After approximately 500 s, the potential returned virtually to its initial value. The laminate generated open-circuit voltage with a peak value of 7.6 $\mu\text{V m}^{-1}$ (normalized to the change in curvature only, as the open-circuit voltage is expected not to depend on the laminate's area) and electric current with a peak value of 0.60 $\mu\text{A m}^{-1} \text{cm}^{-2}$ (normalized to the change in curvature and the area of the free part of the laminate).

Electric charge generated during each bending cycle was obtained by integrating the generated current with respect to time, as depicted in Figure 7H. The laminate was able to generate 1.8 $\mu\text{C m}^{-1} \text{cm}^{-2}$ (normalized to the change in curvature and the area of the free part of the laminate) of electric charge.

The peak voltage and electric current were nearly proportional to the change in laminate's curvature, as depicted in Figure 7B and Figure 7C. Peak current registered at 10 times slower bending speed yielded 30% lower peak value, as depicted in Figure 7C. The electric charge generated in each bending cycle, depicted in Figure 7D, was independent of bending speed.

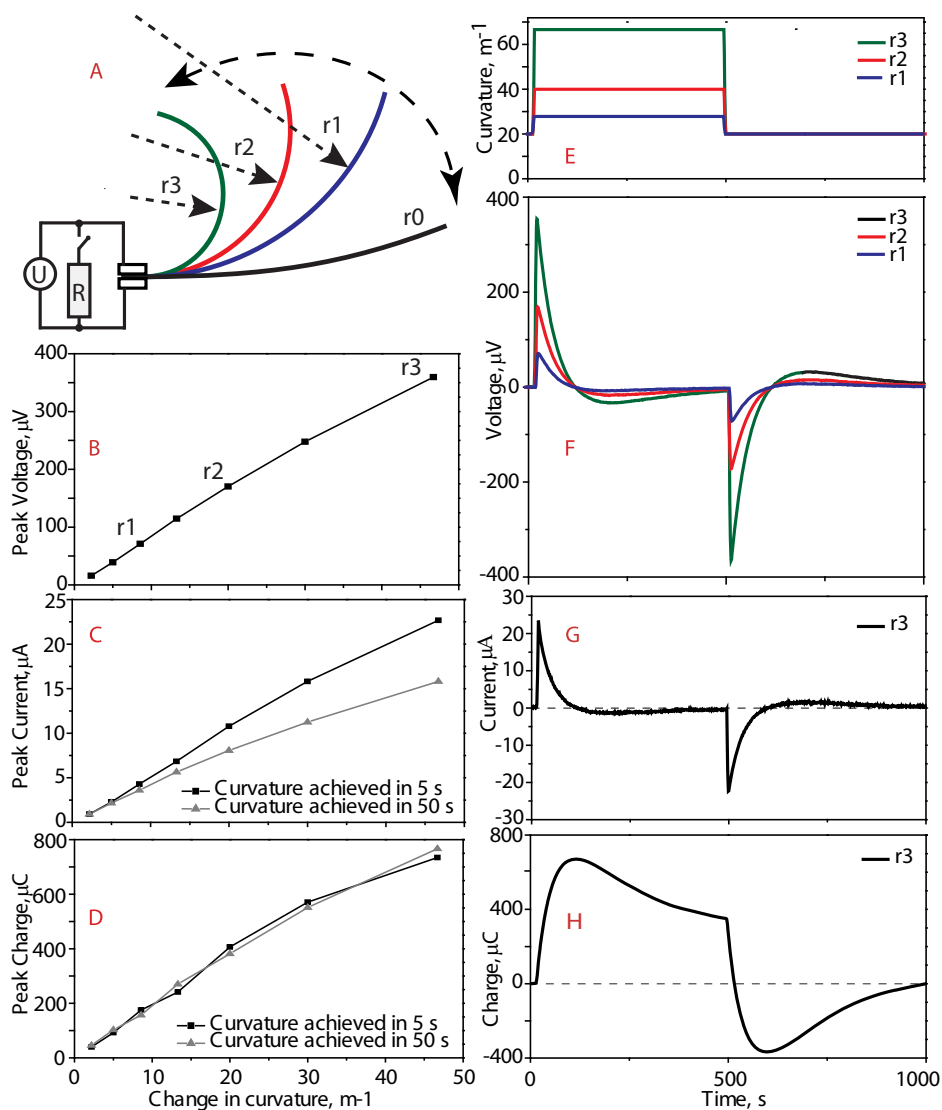


Figure 7. (A) Set-up of voltage and current measurements. (B) Peak voltage value versus final curvature. (C) Peak current value at two bending velocities. (D) Calculated charge values of previous. Transient signals: (E) applied curvatures; (F) corresponding open-circuit voltages; (G) course of short-circuit current; and (H) calculated charge of previous.

5.3 Motion-sensing properties of IEAP Type I

5.3.1 Experiment set-up

Dynamic motion-sensing properties of IEAP Type I were investigated using the Test rig B, as this rig provides sinusoidal bending profile in time and a frequency range wider than that of Test rig A. IEAP was bent at the maximum possible bending amplitude – from -121 to 121 m^{-1} .

The output of the laminate material under test is registered using the National Instruments' PCI-6036E DAQ board. Burr-Brown INA116 instrumentation amplifier was used as preamplifier.

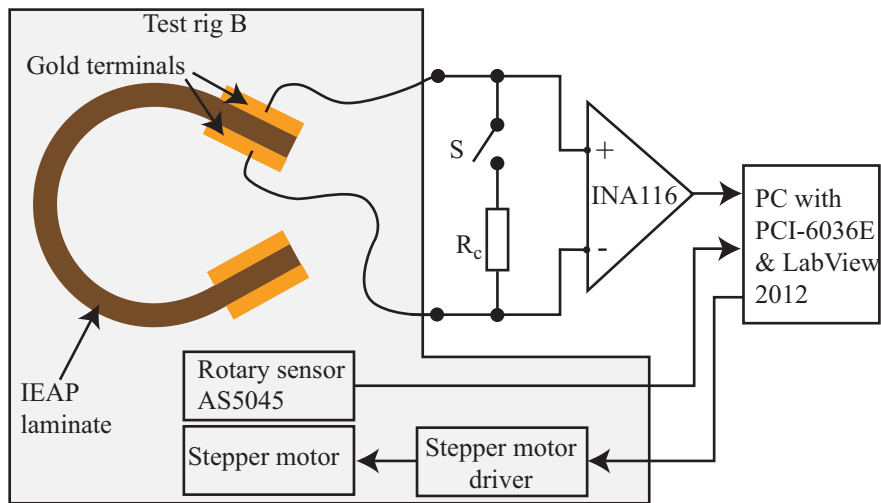


Figure 8. Schematic of the experiment set-up.

Electric current was measured as a voltage drop over a shunt resistor R_c connected between the electrodes, as depicted in Figure 8. The value of the shunt resistor was chosen accordingly to the series resistance of the particular investigated piece of IEAP. If the value of the current-measurement resistor matches the series resistance of the current source (*i.e.* the IEAP), the energy dissipated on the current-measuring resistor is the highest, and the measurements are done at the highest level of accuracy. The actual value of the shunt resistor was 10 or 5 Ω , depending on the particular sample. The same amplifier set-up functions as an ammeter or voltmeter, depending on the state of the switch S , connecting the shunt resistor.

The peak-to-peak values and phase shifts of voltage (U_{pp}) and electric current (I_{pp}) are determined by fitting the measured signal with the sine parameters using a differential evolution algorithm, implemented in National Instruments' LabView environment.

A typical set of transient signals measured at 0.2 Hz bending frequency is shown in Figure 9. The input curvature follows a sinusoidal course. The transient profiles of open-circuit voltage and electric current are also sinusoidal, but their phases lag curvature by 30° at this specific bending frequency. The amount of generated electric charge is determined by integrating the measured electric current with respect to time, as illustrated by the gray area in Figure 9.

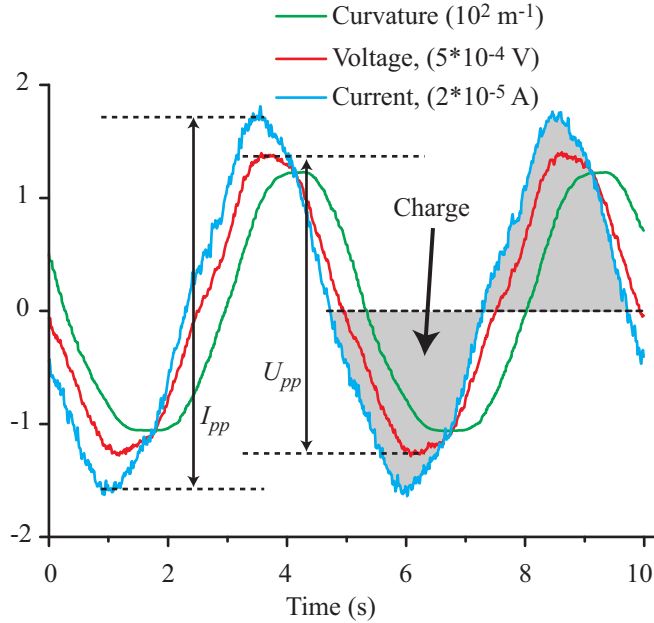


Figure 9. A typical course of transient voltage and electric current of IEAP Type I measured at 0.2 Hz bending frequency. Average generated charge and peak-to-peak values of voltage (U_{pp}) and electric current (I_{pp}) are extracted from the signals.

The size-dependence of IEAP motion sensor output was investigated by measuring the IEAPs of constant length (42 mm), but of different widths (3, 6, 9, and 12 mm). In order to ensure the homogeneity of the parameters of the different samples, the same piece of laminate was cut narrower. The free part of the laminate (the distance between the terminals) was 33 mm; therefore, 21% of the IEAP sheet was rigidly fixed and was not bent. The fixed part acted solely as a supercapacitor.

The experiments were performed at room temperature and at $30 \pm 5\%$ RH.

5.3.2 Frequency-response of IEAP Type I

The transient course of open-circuit voltage after steep bending of IEAP Type I was, in similar to IEAP Type II, discussed in **Section 5.2.2**, characterized by formation of a sharp peak immediately after bending, as depicted in Figure 10A. The subsequent course of open-circuit voltage was notably different – the voltage decreased rapidly, but did not cross its initial (zero) value in the investigated time span.

The significant attenuation of the transient voltage was also expressed in the frequency-dependence of the peak-to-peak voltage value, as depicted in Figure 10B. One order-of-magnitude decrease in the bending frequency resulted in a roughly 12% decrease in the peak-to-peak voltage.

More importantly, the peak-to-peak voltage showed a considerable and irregular dependence on the laminate surface area. This was especially pronounced in the case of the narrowest (3 mm in width) measured sample. This dependence was most likely caused by non-homogeneous surface conductivity due to random discontinuities in the gold current collector. Figure 10C illustrates that a twice-larger laminate sheet resulted in by an approximately 6.0% higher peak-to-peak voltage.

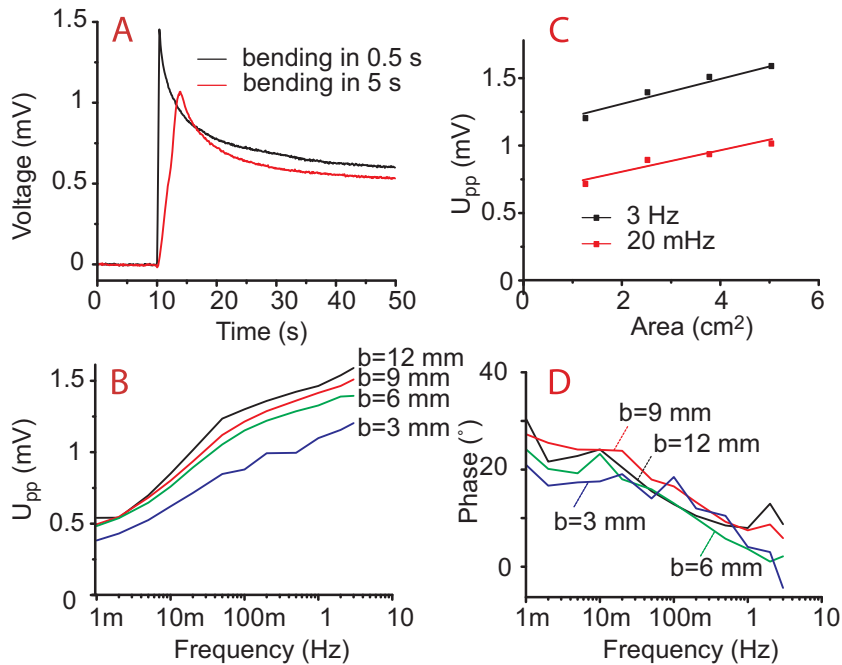


Figure 10. (A) Transient courses of voltage after a change of curvature from -121 to 121 m^{-1} in 0.5 and 5 s. (B) The frequency response of peak-to-peak voltage in the case of IEAPs of different widths. (C) The peak-to-peak voltages as a function of sensor area. (D) The phase shift of voltage.

The phase angle between curvature and open-circuit voltage did not have a pronounced dependence on the laminate area. Open-circuit voltage led curvature change by approximately 25° at 1 mHz and it decreased towards zero with increased frequency, as illustrated in Figure 10D.

The generated electric current was registered as a voltage drop over a $10\text{-}\Omega$ or $5\text{-}\Omega$ resistor; therefore, the measured current does not fully correspond to the ‘real’ short-circuit condition. However, the value of the resistance is in the same range with the internal resistance of the particular laminate.

Similarly to IEAP Type II, the transient course of current in the case of IEAP Type I was characterized by a decay to zero, as depicted in Figure 11A. The gold current collector on IEAP Type I reduced the time needed to discharge the electric charge generated by bending by a factor of 10 – from 100 to 10 s.

Figure 11B demonstrates that the frequency response of peak-to-peak electric current is strongly dependent on frequency, as expected. Theoretically, all parts of the laminate undergoing homogeneous bending motion should give a proportional increase to the total current. Figure 11C confirms that the peak-to-peak current is proportional to the laminate area especially at lower frequencies.

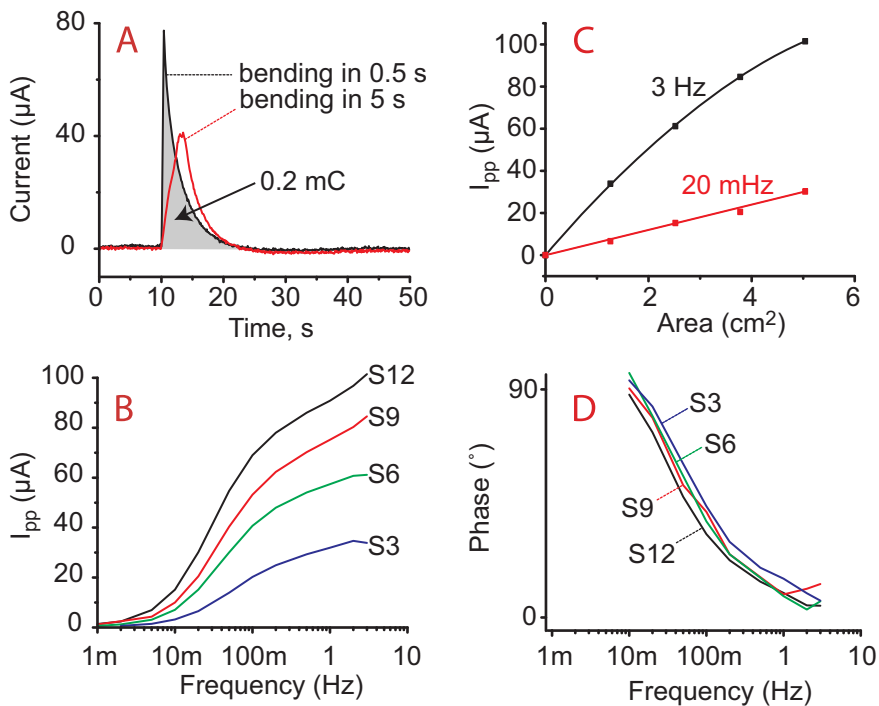


Figure 11. (A) Transient courses of electric current after change of curvature from -121 to 121 m^{-1} in 0.5 and 5 s. (B) Frequency-response of peak-to-peak voltage. (C) Peak-to-peak voltages as a function of sensor area. (D) The phase shift of electric current.

At the frequency <10 mHz, the phase of electric current depicted in Figure 11D led input curvature by nearly 90° , which corresponds to a capacitor-like behavior. The phase shift dropped drastically at higher frequencies.

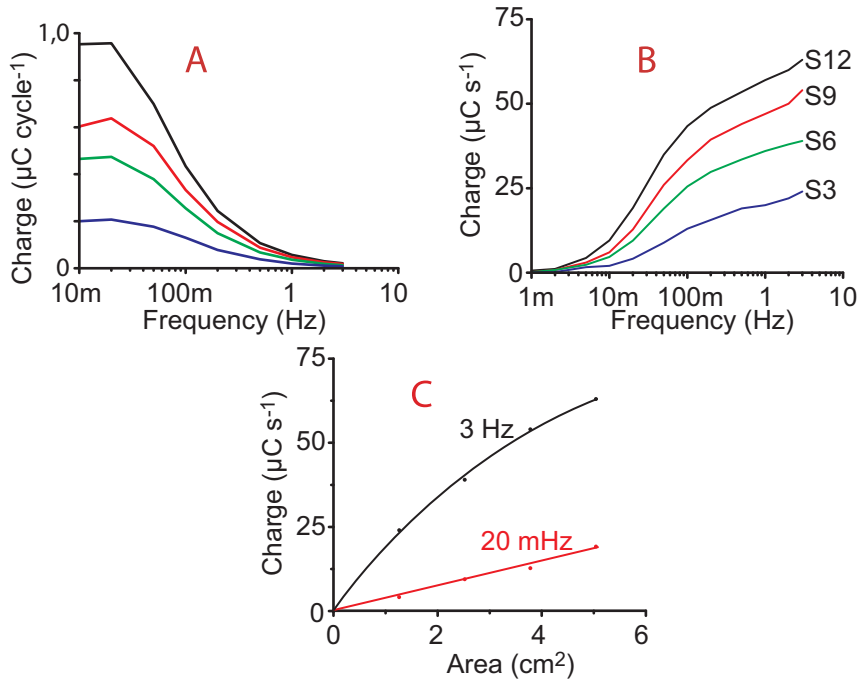


Figure 12. (A) Generated charge per full bending cycle. (B) The generated time-averaged charge. (C) The values for charge at different frequencies as a function of the laminate area.

In the transient analysis provided in **Section 5.2.2**, it was confirmed that the electric charge generated in each bending cycle is independent of the bending speed. In the case of continuous cyclic bending, the electric charge generated in each cycle generally decreased with increased frequency, as illustrated in Figure 12A. Figure 12B proves that more intensive bending (bending at a higher curvature change rate) generated more charge per time. At 3 Hz, the laminate can generate up to $12 \mu\text{C s}^{-1} \text{cm}^{-2}$, as demonstrated in Figure 12C.

5.4 Working principle of IEAP motion sensor

Evolution of the measured open-circuit voltage (Figure 13A) is explained as follows. Initially (Figure 13B), an IEAP is in equilibrium condition, *i.e.* the electric double-layers on the opposite electrodes are equally charged and the voltage between the electrodes is correspondingly equal to zero. After steep

formations of strain difference between the electrodes also hydraulic pressure gradient is formed – the electrolyte is pushed from the compressed electrode towards the stretched-out electrode. In this process, the electrolyte ions in the double-layer are quickly reoriented (Figure 13C). As significant amounts of anions are fixed in the CDC pores, negative potential is formed on the compressed electrode. During reorientation and dislocation of the ions, the double-layer is charged. After diminishing of the hydraulic pressure gradient, the ions in the double-layer reorientate again towards minimum energy. The subsequent behavior of open-circuit voltage is considerably different in the case of the investigated IEAPs Type I and of Type II. In the case of IEAP Type II, the voltage diminished to zero after 100 s (Figure 13D). This point corresponds to the state where the double-layer is the most disturbed from its initial structure. Subsequently, the relaxation becomes the prevalent process and hence a course of voltage with opposite polarity is registered (Figure 13E). In the case of IEAP Type I, the generated voltage decreased more slowly and did not cross the zero value. Finally (Figure 13F), the double-layers in the opposite electrodes have reached a new equilibrium state.

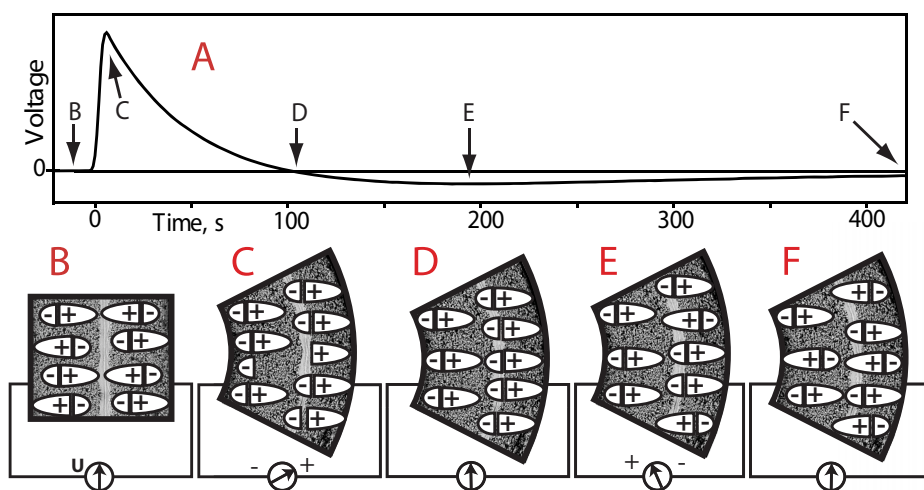


Figure 13. (A) The course of open-circuit voltage and (B-F) the schematic explanation for the formation of the measured voltage.

5.5 Characteristics of the carbon-based IEAP motion sensors

In this work, the IEAPs with activated carbon electrodes are found to operate successfully as motion sensors. Additionally, motion-sensing property has been demonstrated in **Section 5.2** in the case of an IEAP with non-ionic polymer separator (that is, IEAP Type II). The sensorial properties of the IEAPs are compared in Table 5.

Table 5. Parameters for the bending rigs used to investigate motion-sensing properties of the IEAPs

	IEAP Type I	IEAP Type II	Otsuki <i>et al.</i> [64]
Sensor output voltage, $\mu\text{V m}^{-1}$	4.5	7.6	4.9
Attenuation of open-circuit voltage in 10 s	41–48%	20%	15%
Charge output, $\text{mC m}^{-1} \text{m}^{-2}$	1.7	20	

Transient course of voltage generated by the investigated IEAP laminates in response to a steep bending motion was characterized by significant attenuation. The output voltage of IEAP Type II dropped by 20% from its peak value in 10 s, while the voltage on the laminate Type I dropped as much as 41–48% from its peak value in the same time span (Table 5). Attenuation of the output voltage is known also in the case of other carbon-based IEAP motion sensors. Otsuki *et al.* [64] have observed a similar, but less attenuated (attenuation ca 15% of the peak value in 10 s) response in the case of a laminate with IL-impregnated polymer membrane and carbonaceous electrodes.

The investigated IEAP sensors produced open-circuit voltages comparable with the values previously reported by Kamamichi *et al.* [62] and Otsuki *et al.* [64]. Peak output voltage is found to be proportional to the bending magnitude (Figure 7B); therefore, it is possible to measure the magnitude of motion the IEAP is subjected to. On the other hand, large attenuation of the transient signal complicates the measurement of frequent consecutive deformations. Attenuation is also the cause for the nonlinear frequency-response of IEAP motion sensors at constant bending magnitude (Figure 10B). In addition, open-circuit voltage is found to be sensitive to material inhomogeneity. In principle, all parts of the laminate undergoing same bending motion are expected to generate equal voltage. However, a smaller piece of IEAP generated voltage that is considerably lower than that generated by a larger piece, as demonstrated in Figure 10B. Despite substantial difference in the construction method and the composition between IEAP Type I and Type II, their normalized peak output voltages were close in value: when the curvature of an IEAP was changed in 5 s, IEAP Type I

generated $4.5 \mu\text{V m}^1$, while IEAP Type II yielded $7.6 \mu\text{V m}^1$ of peak voltage (Table 5).

Measurement of electric current and charge is shown to be more advantageous in motion sensing. The peak value of electric current was proportional to the bending magnitude, as given in Figure 7C. Every part of the material that is bent uniformly should contribute to the total current and charge in proportion to its area. A linear dependence of the peak current on the laminate area was verified in the case of IEAP Type I, as shown in Figure 11C. As expected, the frequency-response of electric current is highly nonlinear. Figure 11B demonstrates that the current peak value rose with increased frequency up to the highest measured frequency – 3 Hz. At the same time, the phase difference between electric current and mechanical bending also decreased with increased frequency, as demonstrated in Figure 11D.

It is demonstrated that it is possible to measure the magnitude of bending by integrating the generated current, as depicted in Figure 7D. Calculation of the total generated charge is found to provide the most accurate feedback for bending motion. The exceptionally high sensitivity in charge-sensing mode has also been confirmed in the case of IPMC transducers [165].

The value of generated electric charge obtained by this method does not depend on bending speed, enabling accurate measurement of the magnitude of motion. The magnitude of the generated charge varied between different types of IEAP. IEAP Type I yielded $1.7 \text{ mC m}^1 \text{ m}^{-2}$ of charge, normalized against the change in curvature and the laminate area, while IEAP Type II generated as much as $20 \text{ mC m}^1 \text{ m}^{-2}$ of charge (Table 5). A large, 12-fold difference in the charge-generation capacity can be explained by a different amount of active carbon material per laminate area – the thickness of the electrodes of IEAP Type I was $30 \mu\text{m}$, while IEAP Type II had $220\text{-}\mu\text{m}$ electrodes (Table 2). That is, IEAP Type II has roughly 7.3 times more active carbon material for the same surface area, which obviously gives a rise to its charge-generation capacity.

The generated charge provides accurate feedback only if the transient bending profile consists of short bending cycles followed by longer stationary positions. The estimation of magnitude of motion is more difficult in the case of periodic bending. It is shown in Figure 12A that the amount of electric charge generated in each bending cycle decreases with increased frequency. This is caused by the time needed to collect the generated charge from an IEAP, which is approximately 10 s in the case of IEAP Type I, as given in Figure 11A.

The transient courses of voltage and electric current after a steep bending develop as a result of two factors: a) the transient course of electric double-layer charging due to the applied pressure gradient through an IEAP; b) the extraction of the generated charge by a current-measurement device. When the electric current is measured, an IEAP can be seen as a supercapacitor charged by a mechanical stimulus. The discharge circuit for such supercapacitor consists of a series of internal resistance of an IEAP-supercapacitor, a distributed electrode resistance, and a current-measurement resistor.

The results also demonstrate the effect of distributed electrode resistance on the mechanoelectrical parameters of IEAP motion sensors. In the case of IEAP Type I, the electrode resistance is $<1 \text{ } \Omega \text{ square}^{-1}$ due to the high conductivity of its gold current collector. The magnitude of electrical impedance of the electrode of IEAP Type II, which is purely resistive [47], is $28 \text{ } \Omega \text{ square}^{-1}$ (Table 2). In the case of IEAP Type II, the transient courses of voltage and electric current were very similar, which refers to inefficient extraction of the generated charge. In the case of IEAP Type I, a majority of the generated charge was removed in 10 s, as depicted in Figure 11A, which indicates the advantage of using an IEAP with an extra current collector for sensing motion.

6. THE INFLUENCE OF AMBIENT HUMIDITY ON THE ELECTRICAL PARAMETERS OF IEAP

6.1 Introduction

Section 1.3 underlined the significant impact of ambient humidity on the performance of the IEAP materials operating in ambient air. This paragraph investigates experimentally the humidity-dependence of IEAP Type I using electrochemical impedance spectroscopy. The impedance data is fitted with a suitably chosen equivalent electrical circuit and the shift in the equivalent circuit parameters is correlated with the changes in ambient RH.

IEAP Type II contains EMIBF₄ ionic liquid, which undergoes irreversible chemical reactions with water [152]. As the investigation of long-term degradation processes is not in the scope of this thesis, humidity-sensitivity of IEAP Type II is not investigated in this thesis.

The reason for the impedance change at variable ambient humidity is a drift in the material properties due to water vapor, which is reversibly absorbed by an IEAP. The IEAPs used in this work are composed out of highly hygroscopic materials – Nafion, activated carbon, and a hydrophilic IL. Previously, all constituents from this list have been proposed individually for humidity sensing, as it is explained in **Section 4.3**.

The impedance measurement and electromechanical characterization results reveal a number of advantages, but also deficiencies of the increased water content of the laminate.

6.2 Experimental

The impact of ambient RH was investigated by placing the IEAP laminate Type I in a container with a controlled RH value, as depicted on Figure 14. Humidity chambers with five fixed humidity points were constructed. The lowest humidity (0±4% RH) was generated by using calcium chloride (CaCl₂) as absorbent, and the highest humidity value (100±4% RH) settled over a bath of distilled water. The fixed RH values of 23±2, 53±2, and 75±2% RH were generated by using saturated solutions of potassium acetate (CH₃CO₂K), magnesium nitrate (Mg(NO₃)₂), and sodium chloride (NaCl), respectively [166]. All chemicals used for stabilization of the RH level were of technical grade.

The 3-cm² piece of IEAP laminate was fixed between the measurement terminals made of gold. Electric impedance was measured between the IEAP electrodes using PARSTAT 2273 potentiostat in a two-electrode mode. 10 mV RMS signals were used in the measurements.

The IEAP laminate was held in an environment of constant humidity for at least three hours before the impedance measurement for achievement of equilibrium water content in the IEAP. Air convection in the chamber was promoted using an air agitator. During the impedance measurements, the air agitator was turned off. A Rotronic HC2 temperature and humidity sensor was used as a reference for the RH value. All experiments were conducted at room temperature (24±1 °C).

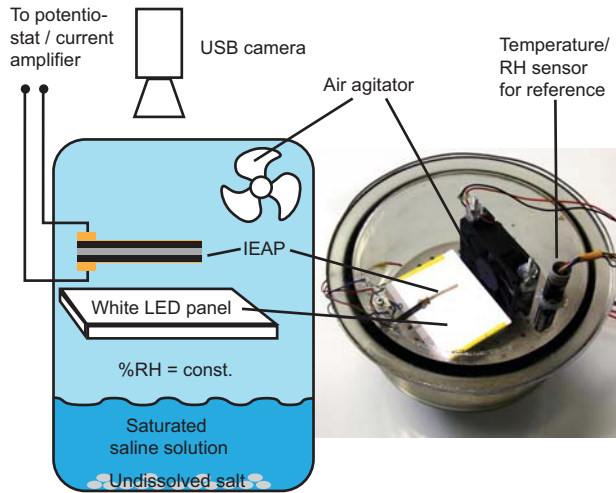


Figure 14. Set-up for impedance measurements.

6.3 Electrical impedance of IEAP at different relative humidities

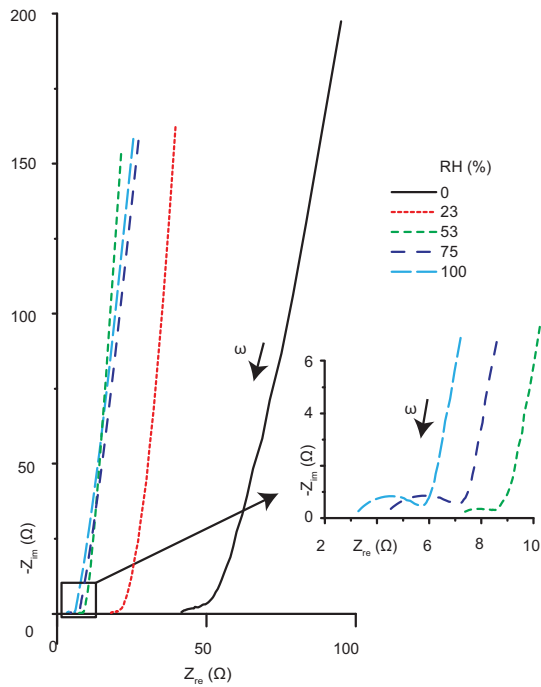


Figure 15. Nyquist plot of IEAP laminate's electrical impedance.

The Nyquist plot of the measured impedance is given in Figure 15A. Impedance of the IEAP changed drastically as a result of changes in the RH level. The most significant difference is the shift of the real part of impedance towards higher values when the RH level was decreased. The IEAP was more sensitive to variation in the RH value in the low (<53%) RH region, while the impedances measured at >53% RH changed only a little.

In the high-RH environment, the Nyquist plot had a characteristic arc-shape at high frequencies (>100 Hz). This arc-shape was not clearly distinguishable at low RH levels. The phase shift between voltage and current was the largest at the lowest RH level, indicating to the least constrained motion of the IL ions.

6.4 Electrical equivalent circuit for an IEAP

Equivalent circuit analysis is an indispensable method to understand the observed changes in the IEAP's impedance. In this work, the equivalent circuit given in Figure 16A is selected to represent an IEAP. Takeuchi *et al.* have previously used a similar equivalent circuit in the modelling of an IEAP actuator with 'bucky gel' electrodes [167].

The equivalent circuit given in Figure 16A consists of three blocks connected in series. Figure 16B gives the physical interpretation for the selected equivalent circuit elements.

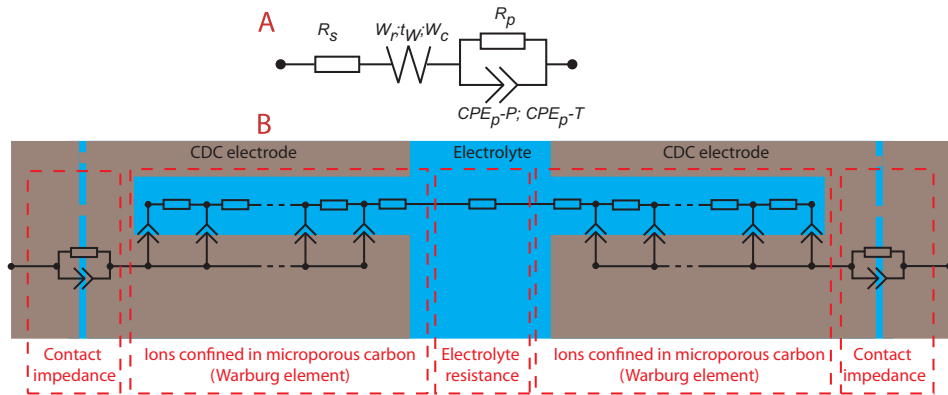


Figure 16. (A)The equivalent circuit for an IEAP and (B) its physical interpretation.

The resistance R_s represents the charge-transfer resistance between the electrodes. The value of R_s is determined by the level of ionic conductivity in the IL-containing polymer membrane.

Warburg element W with a mathematical form given by Equation (1) is a distributed element, which is used to describe the electrochemical systems with anomalous diffusion. The pores in the CDC grains are described as finite transmission lines, as given in Figure 16B. The boundary between the CDC and

the IL electrolyte, *i.e.* the electric double-layer region, is modelled as non-ideal capacitors – constant phase elements. As the mobility of ions inside the pores is considerably constrained, *i.e.* it needs significantly more energy and time to charge the double-layer deep in the pores, a transmission line is formed in the pore thickness direction. A Warburg impedance Z_w is described by three parameters – a proportional parameter W_r ; a frequency-dependent parameter T_w ; and an exponent W_c , which is a measure for non-ideality.

$$Z_w = W_r \frac{\text{cth}[(iT_w\omega)^{W_c}]}{(iT_w\omega)^{W_c}} \quad (1)$$

The last block, which consists of a parallel connection of resistance R_p and a constant phase element CPE_p , represents contact impedances between the CDC grains within each electrode, and the impedance between the electrode and the measurement terminals.

The ionic diffusion constrained by the transmission line effect in the CDC micropores can be presented as a characteristic frequency ω_i , given by Equation (2).

$$\omega_i = \frac{1}{T_w} \quad (2)$$

The impedance spectra, given in Figure 15, were fitted with the equivalent circuit given in Figure 16A. The best-fit values for the seven parameters describing the proposed equivalent circuit were extracted for different humidity levels.

6.5 Impedance analysis results and discussion

Figure 17A demonstrates that a good fit is found for all measured impedances. Figure 17B illustrates that the ionic conductivity of the IL-swollen polymeric membrane increases drastically with increased humidity content. This is also expected, because the conductivity of IL-water mixtures increases with increased water content, until a peak value is achieved. Table 1 indicates that the conductivity of ionic liquid can increase as much as by a factor of six when mixed with water. The electrical conductivity of the IL-containing laminate undergoes drastic changes because of hydration – the resistance R_s decreased with increasing RH level as much as by a factor of 13 – from 41.1 to 3.17 Ω . Consequently, the humidity-sensitivity of IEAP laminate is not governed only by IL.

The magnitude of the distributed resistance – W_r – was constant at the RH levels between 75 and 100%, while it increased 10-fold, from 1.90 to 21.2 Ω , in the dry environment, as given in Figure 17D. This emphasizes a significantly constrained ionic mobility in the dry environment. This is also expressed in a shift of characteristic frequency towards higher values at high RH conditions, as given in Figure 17G.

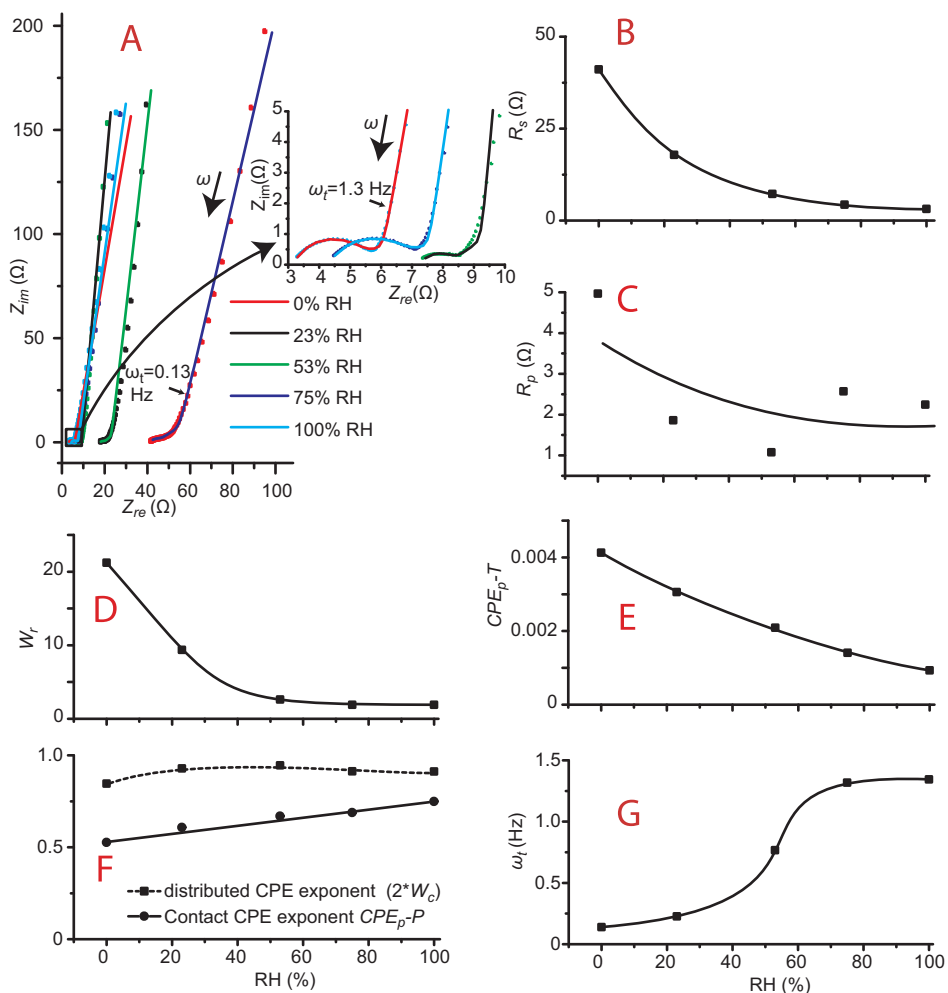


Figure 17. (A) Nyquist plots of impedance with the best-fit curves. (B-F) Best fit parameters of equivalent circuit at different RH levels. (G) Characteristic frequency ω_t at different RH levels.

The exponent of the distributed CPE in the double-layer (equal to $2*W_c$), given in Figure 17F, was in the range of 0.91–0.95 in all RH levels, except in the most hydrated condition. Therefore, the carbon-electrolyte boundary is capacitive in its nature, with only a slight deviation from an ideal capacitor (where $2*W_c \equiv 1$).

The contact impedance has effect only at high (>25 Hz) frequencies, as the CPE is shorted by a low-ohm (1–5 Ω , according to Figure 17C) resistance at lower frequencies. In addition, the contact impedance is more significant in dry environment, as the magnitude of CPE_p-T drops by a factor of 4.4 with increased RH, according to Figure 17E. In addition, the CPE_p-P is equal to 0.53 at the lowest RH (Figure 17F), which refers that, in addition to electronic

current, there is also a significant amount of ionic current between the different regions within a single electrode.

The impedance analysis results suggest that it is possible to measure the RH value over an IEAP laminate by registering impedance between its electrodes. In Figure 18, the possibility of measuring the RH value by registering the phase difference between applied voltage and measured current is demonstrated. The phase change is linear at RH values >23%. More importantly, the magnitude of phase change is large (in tens of degrees), which enables measurements of RH value with high accuracy. The measurement of the RH value by registering the impedance of the same material is advantageous, because the signal directly corresponds to the momentary humidity content of the laminate. An external humidity sensor, based on a different active material, can also have different humidity-absorption kinetics. If the RH value, extracted using an external sensor, would be used as a calibration parameter for an IEAP as a motion sensor, it can result in a considerable inaccuracy.

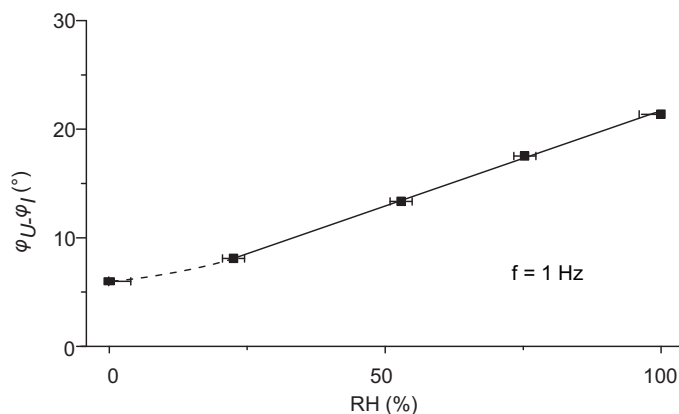


Figure 18. The extraction of the RH value by measuring the phase angle at 1 Hz.

As a conclusion, the absorbed water content influences the electrical properties of IEAP laminates and the ambient RH level should therefore be considered in development of applications for IEAP as an actuator, a sensor, or a super-capacitor. Additionally, the humidity-sensing capability broadens the field of application of IEAPs, as an IEAP performing any other function in a device can additionally sense the RH level.

In addition to the electrical properties, it should be considered that also the mechanical properties of IEAP change considerably in an environment of variable RH level. The investigation of the relation between the mechanical properties and the RH level is out of the scope of this thesis.

7. IEAP AS A HYGROELECTRICAL SENSOR

As demonstrated in **Section 6**, the electrical impedance of an IEAP laminate is highly dependent on the ambient RH value. It is therefore possible to determine the RH value around an IEAP laminate by measuring its electrical impedance. This is an advantageous and unique additional feature for IEAP, primarily engaged as either an actuator or a supercapacitor. The use of an IEAP primarily as an impedance-based humidity sensors is, however, impractical due to the relative complexity of the three-layered laminate and a wide choice of highly-developed competitive (*e.g.* resistive, capacitive, or quartz crystal microbalance-based) humidity sensor technologies.

The use of changes in the IEAP's impedance in humidity sensing is well predictable, concerning its highly hygroscopic constituents. In this work, humidity-sensitivity of IEAP is found to be expressed in one additional, unanticipated way. The newly found sensing phenomenon reveals itself in formation of voltage and electric current between the IEAP electrodes, when the opposite electrodes of an IEAP laminate are exposed to an environment with uneven RH distribution. In other words, a humidity gradient across an IEAP results in formation of a macroscopic electric charge. Concurrently, volumetric effects emerge; *i.e.* the side of laminate exposed to a higher RH expands and the cantilevered laminate bends towards the drier environment. The bipartite response of an IEAP laminate is demonstrated in Figure 19.

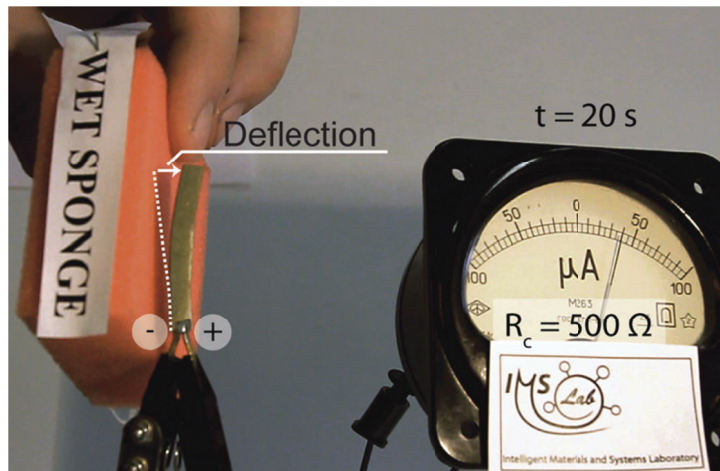


Figure 19. Demonstration of the humidity response of a cantilevered piece of IEAP Type I.

7.1 Set-up for measurement of hygroelectrical properties

The water sorption-induced charge-generation properties were characterized by exposing the opposite sides of an IEAP Type I laminate to chambers, which have fixed RH values. An IEAP laminate was fixed between epoxy frames, as illustrated in Figure 20A. The ‘windows’ in the plates with an IEAP between them were exposed to the humidity chambers. The constant RH levels in the humidity chambers were established by the use of saturated saline solutions, in similar to the experiments described in **Section 6.2**.

Before the experiments, the humidity content in an IEAP was equilibrated by exposing the opposite sides of the laminate to humidity chambers with equal RH, as illustrated in Figure 20C. Subsequently, one humidity chamber was replaced quickly (in ~ 1 s) with a humidity chamber with a different RH level, as depicted on Figure 20D, consequently establishing a RH gradient across IEAP. All humidity chambers were equipped with air agitators, which ensured preservation of constant RH in the chambers and also accelerated the water sorption or desorption.

Voltage and electric current were registered using a National Instruments PCI-6036E DAQ board. The bias current of the PCI-6036E DAQ board with its SCC-AI series front-end analog input modules was found to be too high (about 10 nA) for measurement of open-circuit potential on capacitor-like systems, as the capacitor under test is charged by the current originating from the measurement device in the long run. Therefore, a preamplifier with low input bias current is needed. Burr-Brown INA116 instrumentation amplifier with an extremely low input bias current (< 3 fA) was selected as a preamplifier.

Electric current was measured as a voltage drop over a low-ohm resistor, as depicted in Figure 20B. The same amplifier set-up was used as an ammeter or a voltmeter, depending on the state of the switch S, connecting the shunt resistor. The actual value of the shunt resistor – 10Ω – was equivalent to the value of series resistance R_s at medium RH level, as given in Figure 15 for a similar IEAP of comparable size. Matching the internal resistance R_i with the value of the shunt resistor R_c assured that the power dissipated on the shunt resistor R_c was the highest.

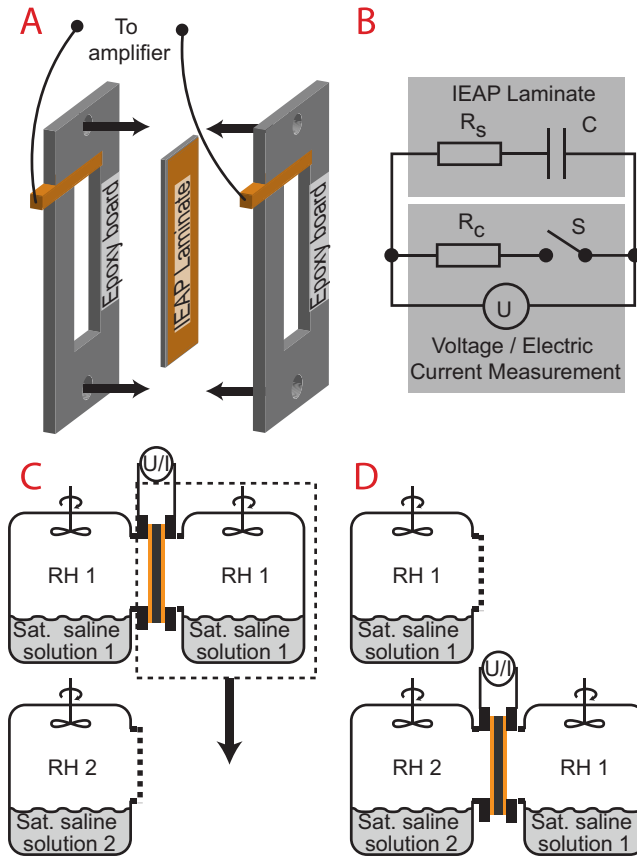


Figure 20. (A) Fixing of an IEAP between epoxy plates with ‘windows’. (B) The set-up for electrical measurements. (C-D) The experiment set-up for varying RH gradient across an IEAP.

7.2 Transient response to humidity gradient

7.2.1 Open-circuit voltage

The transient course of open-circuit voltage after a sudden formation of a RH gradient across IEAP revealed two different processes with different time constants, as depicted in Figure 21. Immediately after formation of humidity gradient, the voltage rose steeply and gained its peak or ‘knee’ in 100–500 s. After this, the open-circuit voltage increased further and achieved its final peak after as long as 2.2 h.

The process with a shorter time constant corresponds to water sorption or desorption processes occurring in this particular electrode, above which the RH was changed. Concurrently, also water diffusion through IEAP slowly starts to occur. After the time of a first peak or a ‘knee’ value in 100-500 s, water diffu-

sion across IEAP becomes the primary mechanism, responsible for increasing the open-circuit voltage.

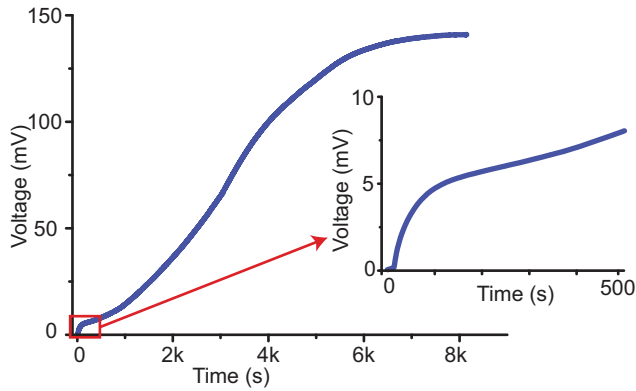


Figure 21. Transient course of the open-circuit voltage after exposing an initially dry electrode to 50% RH.

Synchronously to the rise of open-circuit voltage across IEAP laminate, also volumetric effects emerged. Figure 22 illustrates the course of open-circuit voltage in comparison with the deflection of a cantilevered IEAP as a response to a RH increase above one of the electrodes. In this experiment, the IEAP laminate was not fixed between the rigid plates. This enabled measurement of the bending motion using a laser displacement meter, but, in turn, complicated the estimation of the humidity gradient magnitude across the IEAP.

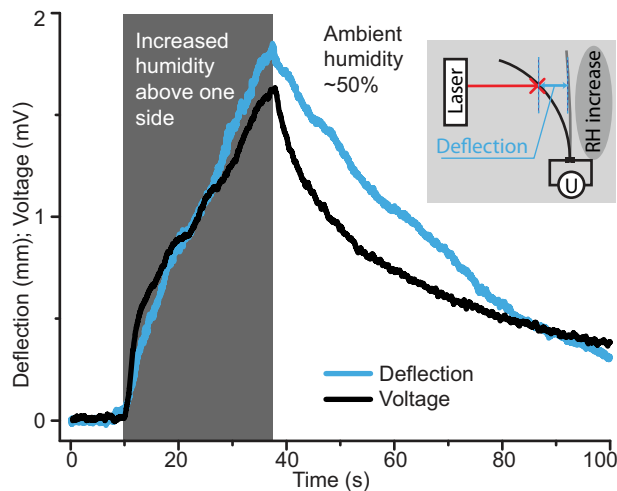


Figure 22. Simultaneous deflection of a cantilevered IEAP laminate and formation of an open-circuit voltage between the electrodes after formation of a humidity difference between the electrodes.

The open-circuit voltage was clearly more sensitive, compared to deflection, to the change (to both increase and decrease) in RH above the laminate. Bending of the laminate reflects the total strain in all parts of the laminate; therefore, it is obvious that the diffusion of absorbed water through the electrode needs a significant amount of time. On the contrary, sorption of water by even the topmost layer of a single electrode can be registered by measuring the voltage difference between the electrodes.

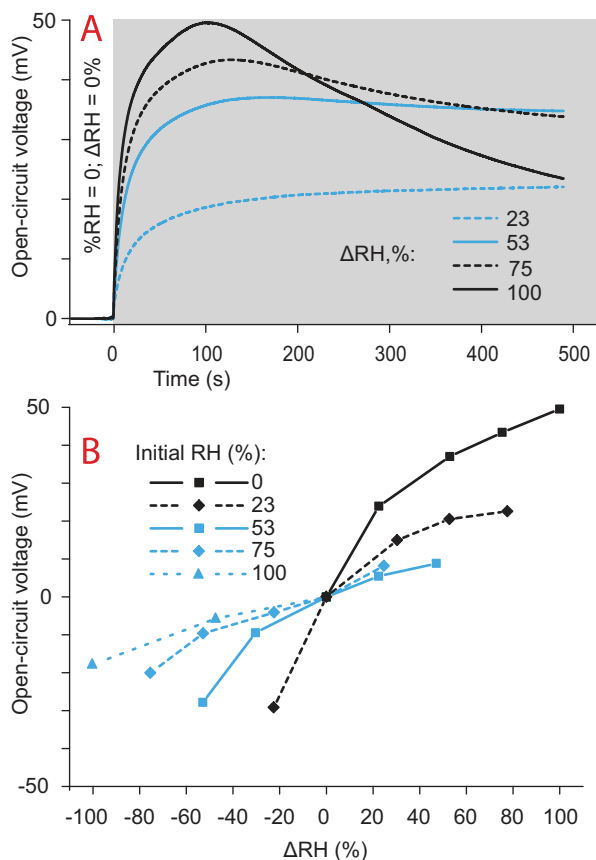


Figure 23. (A) Transient course of the voltage after initially dry electrodes were exposed to different levels of humidity. (B) Peak values of open-circuit voltage for all tested combinations of initial humidity and humidity gradients.

The transient course of voltage was characterized by a steep rise of voltage immediately after the formation of RH gradient, gaining its peak value in 100-500 s. As expected, the peak or ‘knee’ value was dependent on the magnitude of RH gradient, as illustrated in Figure 23A.

Figure 23B shows the peak values of open-circuit voltages (in the case a peak value was not formed in 500 s, the open-circuit value after 500 s is given) measured in experiments with various combinations of initial equilibrium RH values and induced RH gradients. The RH gradient positive by its sign refers to the experiment where the RH gradient was achieved by increasing the RH level, and *vice versa*. It was observed that (a) smaller increase in RH gradient yields proportionally larger open-circuit voltages; and (b) RH increase yielded higher peak values, as absorption process is generally faster than desorption.

The transient course of electric current after the formation of RH gradient was characterized by a steep peak and subsequent decay. Figure 24A shows that the level of electric current dropped to the electrical noise level after 150 s. The peak value of electric current was roughly proportional to the change in RH level, as illustrated in Figure 24C, on the assumption of an equal initial humidity level. At the same time, the slope between peak value of current and the change in RH was strongly dependent on the initial RH level. Interestingly, the generated values of electric charge, calculated in Figure 24B for transient courses given in Figure 24A, did not follow the same trend with peak current – the RH gradient of 100% yielded roughly the same amount of charge as the gradient of 75%.

In the conducted experiments, the laminate was returned to initial, homogeneous RH after 300 s. The repeated change in RH caused a second peak of electric current to be formed; only the direction of current was reversed this time. The peak values are given in Figure 24D for all investigated combinations of initial RHs and RH gradients. It can be noticed that the peak corresponding to the return to initial conditions did not follow the same pattern with the peak formed after the initial disturbance of RH level. Figure 24A illustrates that the highest peak was formed when one side of the initially dry laminate was exposed to the highest RH, but the return to the initial conditions yielded the lowest peak value instead.

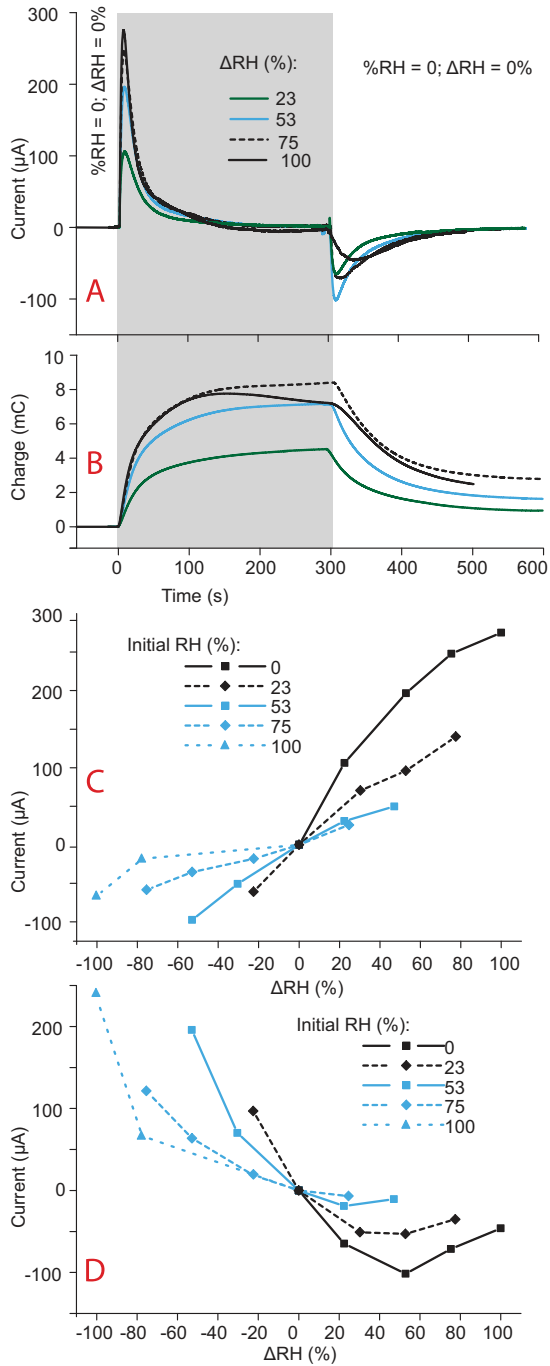


Figure 24. (A) Transient response of electric current to humidity change. (B) Generated and stored charge as a function of time. (C) Peak values of the electric current at various combinations of initial humidity and humidity gradients. (D) Peak values of the electric current upon returning the laminate to the initial humidity levels.

7.2.2 Cyclic stability

The electrical output of IEAP laminate in response to ambient humidity gradient has a high cyclic stability. In the cycling experiment, depicted in Figure 25A, the laminate was placed between the humidity chambers with 0 and 53% RH and the humidity gradient was reversed after every minute. After 1000 cycles, the transient course of open-circuit voltage was nearly indistinguishable from the initial. The charge generated in each cycle, however, showed a small decrease – the 1000th cycle yielded 92% of the charge generated in the first cycle, as depicted in Figure 25B.

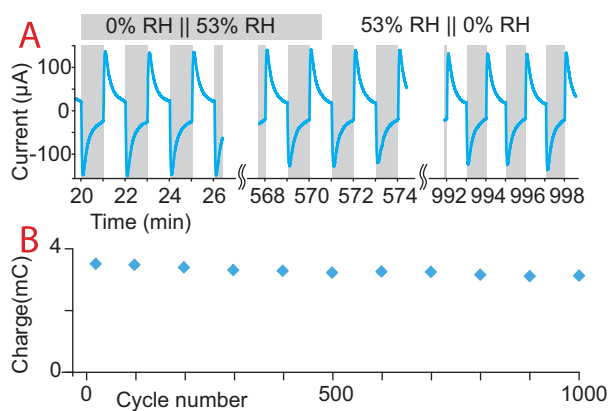


Figure 25. (A) Output current of the laminate during the cycling test. (B) Variation of the generated charge in consecutive cycles.

8. IEAP AS AN ENERGY HARVESTER

IEAP laminates can convert mechanical and water-sorption energy into electrical; therefore its energy harvesting capability is a topic of interest.

IEAP generates electric charge as a result of mechanical stimuli, but the magnitude of the generated charge is low. The highest transient electric power generated by IEAP Type II as a response to mechanical bending has been found to be 0.4 nW cm^{-2} in the case of an impedance-matched load [151]. This power level is evidently too low to be considered for energy harvesting. Consequently, energy harvesting only from ambient humidity is considered in this thesis.

8.1 IEAP for hygroelectrical energy harvesting

The voltage and electric current generation from ambient RH gradient by the use of an IEAP material is discussed in **Section 7.2**. This paragraph characterizes the use of IEAP laminates as hygrovoltaic cells for hygroelectrical energy harvesting.

The highest charge generation rate occurs directly after the change of RH. In principle, the highest momentary charge output of $1500 \text{ C m}^{-2} \text{ h}^{-1}$ or $3300 \text{ C kg}^{-1} \text{ h}^{-1}$ was registered; although, at the lowest voltage ($<1 \text{ mV}$), which is impractical to be used to power any electronic device.

As described in **Section 7.2.1**, the open-circuit voltage on an IEAP increases when the laminate is held between environments with different RHs. An IEAP is able to produce a small amount of electric current from water diffusion through the laminate. This amount of current is too low to be collected by any external power-conditioning circuitry. At this point, the capacitive properties of IEAP come into use. IEAP is able to store a significant amount of generated electric charge in the very same material, where the charge was generated.

In conventional energy harvesting systems, the generated electric energy is transferred into intermediary storage units via power-conditioning circuitry. The power-conditioning electronics start to work only if the input current or voltage has increased over some threshold level. In the case of an IEAP hygroelectrical cell, external power-conditioning electronics is not required; therefore, it can harvest energy at any rate. Consequently, energy can be harvested from sources previously considered unavailable.

The total amount of energy collected into an IEAP during a long (from hours to days) time span can be extracted, on demand, at very high rate. This energy-consumption profile matches with the WSN nodes, which operate at low-duty-cycle mode.

Figure 26 describes the use of IEAP as an energy harvester. IEAP Type I was held between humidity chambers with different RHs during more than 2 hours, until the open-circuit voltage achieved its peak value. Subsequently, the IEAP was discharged on a $10\text{-}\Omega$ load R_c , which was connected between the IEAP electrodes via switch S . The resistor R_c simulated an electronic device

consuming the charge in a real-world application. Only 30 s was needed to discharge the IEAP fully. More importantly, the peak current of 23 A m^{-2} was registered, which corresponds to a power density of 2.0 W m^{-2} . This current level is as much as 31 times higher than the highest peak current registered in continuous mode directly after a rapid change of RH gradient. The difference in power density is even more drastic – by the use of periodic charge-discharge cycle, the peak power density increased as much as three orders of magnitudes, from 2.1 mW m^{-2} to 2.0 W m^{-2} .

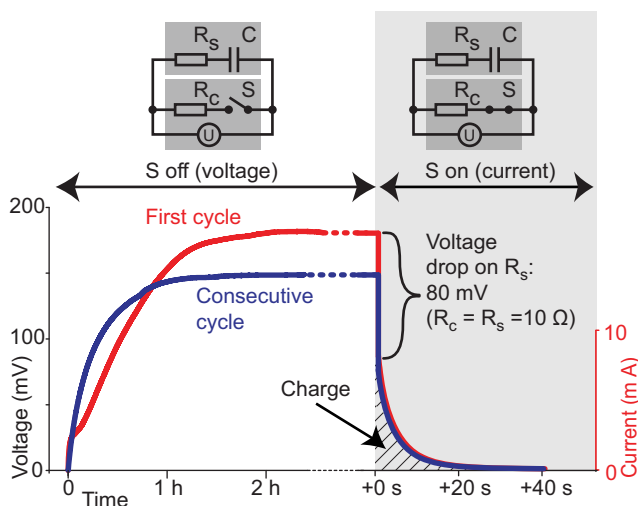


Figure 26. Energy harvesting principle based on intermittent charging and discharging of the capacitive IEAP laminate.

The highest energy density of the hygroelectrical energy harvester was 4.4 J m^{-2} . As a comparison, the same IEAP working purely as a supercapacitor, with a nominal voltage of 3 V and capacitance of 270 F m^{-2} , can hold 810 C m^{-2} of charge and it has an energy density of 1215 J m^{-2} . Therefore, the laminate is able to collect up to 6% and 0.36% of its maximum charge and energy, respectively, merely from ambient humidity.

The simultaneous energy-storage capability is a unique property among energy-harvesting materials. For a comparison, a metallized $17 \text{ }\mu\text{m}$ thick film of crystalline PVdF is able to collect 0.5 J m^{-2} of energy from human respiration in 20 minutes [89]. At the same time, the energy-harvesting material itself as a parallel plate capacitor with a relative permittivity $\epsilon_r = 11$ can hold only 7.3 mJ m^{-2} , when charged to 10 V . The energy generated in each cycle has to be collected into external storage units for subsequent use. Therefore, an IEAP material can collect energy from merely humidity gradients with a rate that is comparable to mechanical stimulus. Moreover, there is no need for external energy storage units, as the material itself can store a significant amount of energy.

9. CONCLUSIONS

The work at hand explored a novel and distinctive characteristic of the IEAP laminates with high specific surface area activated carbon electrodes – the IEAPs respond to various externally imposed stimuli by formation of electric charge between the electrodes.

In the first part of this work, IEAP laminate's response to mechanical bending was investigated. The IEAPs with IL as electrolyte and both ionic and non-ionic polymer as separator were considered. The transient response of IEAPs to bending motion was characterized by formation of a sharp peak immediately after bending and slow diminishing of the generated voltage and electric current towards zero. IEAP motion sensor had a strongly nonlinear frequency response. However, it is possible to determine the magnitude of infrequent bending action by measuring electric current between the electrodes.

In addition to their motion-sensing capability, IEAP laminates were found to have remarkable sensitivity to ambient humidity. Impedance spectroscopy analysis revealed that the series resistance decreased as much as 13 times because of RH change above the laminate. This is caused by highly hygroscopic constituents of the investigated IEAP laminates. The use of an IEAP as a sensor for measurement of ambient RH level was demonstrated.

The most significant novelty in this work is engagement of the IEAP's strong response to the ambient water vapor in a novel, previously unconceived configuration. It was discovered that IEAP laminate responds not only to uniform RH level, but also to RH gradient. Establishment of a unidirectional humidity gradient across IEAP laminate resulted in formation of electric current and voltage between its electrodes – an IEAP serves as a hygrovoltic cell. What is the most remarkable; the magnitude of the generated electric charge because of RH gradient was found to be more than an order of magnitude higher than the electric charge generated as a result of mechanical bending. The high magnitude of the generated charge suggested that the field of application for IEAPs could be broadened towards hygroelectrical energy harvesting. Consequently, IEAP technology can bring ambient humidity gradient among the available sources for harvesting electrical energy.

In hygroelectrical energy harvesting, the supercapacitor-like properties of IEAP laminates are brought into use. An IEAP hygrovoltic cell is able to store the generated electric charge into itself, therefore serving concurrently as an energy harvester and a storage unit. This property enables collection of electric energy from the environment during a long time at a low rate, and extraction of the total harvested energy at a high rate.

Formation of electric charge because of mechanical stimuli and water vapor absorption have a similar underlying physical mechanism. Charge formation can occur if the following preconditions are met:

- a) Unequal conditions are applied to the opposite electrodes of a single laminate. In the case of mechanoelectrical transduction, the opposite electrodes of a bent laminate are exerted to unequal mechanical stress; and in

the case of hygroelectrical transduction, different conditions on the opposite electrodes are achieved by varying the environmental conditions above them.

- b) The mobility of cations and anions in the carbon and polymer matrix are unequal. This is achieved by tailoring of the porosity parameters of the IEAP electrode and the morphology of the ionically conductive polymeric separator.

IEAPs are demonstrated to be multifunctional materials. In addition to their sensorial properties, virtually the same IEAP laminates as investigated in this work can function also as electromechanical actuators and as supercapacitors for energy storage.

10. SUMMARY IN ESTONIAN

Süsinikmaterjalist elektroodidega ioonsed ja mahtuvuslikud elektroaktiivsed laminaadid sensorite ning energiakogumisseadmetena

Ioonsed elektroaktiivsed polümeerid (IEAP) on laminaatmaterjalid, mis koosnevad suure-eripinnalistest elektroodidest, elektroode eraldavast mikropoorsest polümeersest membraanist ning elektrolüüdist, mis sisaldub nii polümeermembraanis kui ka elektroodides. IEAP-d on multifunktsionaalsed materjalid – varasemalt on IEAP-d tuntud eelkõige energiasalvestuselementide ning elektromehaaniliste täituritena. Käesolev doktoritöö uurib suure-eripinnaliste süsinik-elektroodidega IEAP-laminaatmaterjali uudset ja unikaalset omadust – võimet tekitada elektrilaengut mitmesuguste väliste mõjurite toimel.

Doktoritöö esimeses osas uuritakse eksperimentaalselt IEAP elektrilist kostet välise jõu abil painutamisele. IEAP-laminaadi painutamine toob kaasa nii elektripinge kui -voolu piikväärtuse tekke elektroodide vahel. IEAP-painutus-sensori sageduskoste on tugevalt mittelineaarne. Doktoritöös on demonstree-ritud, et on võimalik mõõta perioodiliselt toimuvate painutuste ulatust, registreerides elektrivoolu teket elektroodide vahel.

Töö käigus uuriti IEAP-sid, mis sisaldavad elektrolüüdina ionvedelikku ning on seetõttu võimelised töötama õhu käes praktiliselt piiramatul ajajooksul. Vaatamata ionvedeliku mitteaurustumisele leiti aga, et IEAP elektrilised omadused on erakordselt tundlikud ümbritseva keskkonna suhtelise õhuniiskuse suhtes, sest laminaadi kõik koostisosad on hügrooskoopsed. Töös demonstree-ritakse keskkonna suhtelise õhuniiskuse määramist IEAP-laminaadist sensori abil.

Antud doktoritöö kõige olulisem uudsus on IEAP niiskustundlikkuse rakendamise varasemalt tundmatus konfiguratsioonis. Töö käigus avastati, et IEAP reageerib lisaks suhtelise õhuniiskuse muudule ka õhuniiskuse gradiendile. Niiskuse gradiendi püstitumine IEAP-laminaadi vastaskülgedele vahel tingib elektripinge ja -voolu tekke elektroodide vahel – IEAP käitub hügroelektrilise rakuna. On tähelepanuväärne, et õhuniiskuse gradient, võrrelduna välise jõu abil painutamisega, suudab IEAP-laminaati laadida enam kui ühe suurusjärgu võrra kõrgemale laetusastmele. Genereeritava laengu suur hulk viitab, et IEAP-laminaadi perspektiivseks uudseks kasutusalaaks võib olla hügroelektriline energiakogumine. IEAP-laminaat on ühtlasi üks väheseid olemasolevaid seadmeid, millega on võimalik õhuniiskuse sorptsiooni energiat muundada otseselt elektrienergiaks.

IEAP-laminaadi rakendamisel hügroelektrilise energiakogumisseadmena on olulise tähtsusega tema kondensaatoromadused. IEAP hügroelektriline rakk on võimeline salvestama genereeritud elektrilaengu samasse materjali, mis antud laengu genereeris. See omadus teeb võimalikuks elektrienergia kogumise vähesel määral väga pika aja jooksul ning vajaduse tekkimise korral kogu IEAP-sse talletatud elektrienergia väga kiire väljavõtmise. Antud töös

registreeriti õhuniiskuse gradiendi toimel IEAP-sse salvestatud energia maha-laadimisel maksimaalne voolutugevus 23 A m^{-2} .

Elektrilaengu teke omab sarnast füüsikalist mehhanismi nii paindumise kui õhuniiskuse gradiendi tekke tagajärjel. Elektrilaeng saab IEAP elektroodidel formeeruda juhul, kui on samaaegselt rahuldatud alljärgnevad eeltingimused.

- a) IEAP vastaselektroodid satuvad erinevatesse tingimustesse. Liigutussensorina kasutamise korral rakendatakse IEAP vastaselektroodidele erinev mehaaniline pinge ning hügroelektrilise raku korral tekitatakse erinevad tingimused ümbritseva keskkonna parameetrite muutmise teel.
- b) Katioonide ning anioonide mobiilsus süsinikelektroodides ning polümeerses maatriksis on erinev. Erinev mobiilsus saavutatakse erineva poorsusjaotusega elektroodimaterjali kohaldamise ja ioonjuhtiva polümeerseparaatori valiku teel.

Süsinikelektroodidega IEAP-materjalid on äärmiselt multifunktsionaalsed. Käesolevas töös demonstreeritakse, et lisaks varasemalt tuntud rakendustele energiasalvestuselemendi ning täiturina funktsioneerivad sisuliselt samad IEAP-laminaadid ka liigutussensori, niiskussensori ning hügroelektrilise energia-kogumiselemendina.

II. REFERENCES

- [1] S. Kim, C. Laschi, B. Trimmer, Soft robotics: a bioinspired evolution in robotics, *Trends Biotechnol.* 31 (2013) 287–294.
- [2] T. Someya, *Stretchable Electronics*, Wiley, Weinheim, 2012.
- [3] H. Koo, O.D. Velev, Ionic current devices – Recent progress in the merging of electronic, microfluidic, and biomimetic structures, *Biomicrofluidics.* 7 (2013) 031501.
- [4] H. Zheng, Y. Liu, Z. Chen, Fast motion of plants: From biomechanics to biomimetics, *Journal of Postdoctoral Research.* 1 (2013) 40–50.
- [5] F. Béguin, V. Presser, A. Balducci, E. Frackowiak, Carbons and Electrolytes for Advanced Supercapacitors, *Adv Mater.* 26 (2014) 2219–2251.
- [6] M.J. Park, I. Choi, J. Hong, O. Kim, Polymer electrolytes integrated with ionic liquids for future electrochemical devices, *J Appl Polym Sci.* 129 (2013) 2363–2376.
- [7] V. Presser, M. Heon, Y. Gogotsi, Carbide-Derived Carbons – From Porous Networks to Nanotubes and Graphene, *Adv Funct Mater.* 21 (2011) 810–833.
- [8] O. Kim, T.J. Shin, M.J. Park, Fast low-voltage electroactive actuators using nanostructured polymer electrolytes, *Nat Commun.* 4 (2013) 2208.
- [9] H.I. Becker, Low voltage electrolytic capacitor (US2800616), issued 07/23/1957.
- [10] J. Miller, A brief history of supercapacitors, *Battery Energy Storage Technology.* (Autumn 2007) 61–78.
- [11] E.F. François Béguin, *Supercapacitors: Materials, Systems, and Applications*, Wiley, Weinheim, 2013.
- [12] H. Kurig, Electrical double-layer capacitors based on ionic liquids as electrolytes, *Dissertationes Chimicae Universitatis Tartuensis* 112, Tartu University Press, Tartu, 2011.
- [13] Y. Li, R. Torah, S. Beeby, J. Tudor, An all-inkjet printed flexible capacitor for wearable applications, *Design, Test, Integration and Packaging of MEMS/MOEMS (DTIP), 2012 Symposium on.* (2012) 192–195.
- [14] J. Ren, W. Bai, G. Guan, Y. Zhang, H. Peng, Flexible and Weaveable Capacitor Wire Based on a Carbon Nanocomposite Fiber, *Adv Mater.* 25 (2013) 5965–5970.
- [15] K. Jost, G. Dion, Y. Gogotsi, Textile energy storage in perspective, *J Mater Chem A.* (2014), (Advance Article; DOI: 10.1039/C4TA00203B).
- [16] H. Cheng, Z. Dong, C. Hu, Y. Zhao, Y. Hu, L. Qu, N. Chen, L. Dai, Textile electrodes woven by carbon nanotube–graphene hybrid fibers for flexible electrochemical capacitors, *Nanoscale.* 5 (2013) 3428–3434.
- [17] Y. Fu, X. Cai, H. Wu, Z. Lv, S. Hou, M. Peng, X. Yu, D. Zou, Fiber Supercapacitors Utilizing Pen Ink for Flexible/Wearable Energy Storage, *Adv Mater.* 24 (2012) 5713–5718.
- [18] S. Lee, K. Choi, W. Choi, Y.H. Kwon, H. Jung, H. Shin, J.Y. Kim, Progress in Flexible Energy Storage and Conversion Systems, with a Focus on Cable-Type Lithium-Ion Battery, *Energy Environ.Sci.* 6 (2013) 2414–2423.
- [19] L. Hu, Y. Cui, Energy and environmental nanotechnology in conductive paper and textiles, *Energy Environ Sci.* 5 (2012) 6423–6435.
- [20] X. Cai, M. Peng, X. Yu, Y. Fu, D. Zou, Flexible Planar/fiber-architected Supercapacitors for Wearable Energy Storage, *J.Mater.Chem.C.* 2 (2013) 1184–1200.

- [21] L. Hu, M. Pasta, F.L. Mantia, L.F. Cui, S. Jeong, H.D. Deshazer, J.W. Choi, S.M. Han, Y. Cui, Stretchable, porous, and conductive energy textiles, *Nano Lett.* 10 (2010) 708–714.
- [22] D. Wei, T.W. Ng, Application of novel room temperature ionic liquids in flexible supercapacitors, *Electrochem Commun.* 11 (2009) 1996–1999.
- [23] M.F. El-Kady, V. Strong, S. Dubin, R.B. Kaner, Laser scribing of high-performance and flexible graphene-based electrochemical capacitors, *Science*. 335 (2012) 1326–1330.
- [24] M. Beidaghi, Y. Gogotsi, Capacitive energy storage in micro-scale devices: Recent advances in design and fabrication of micro-supercapacitors, *Energy Environ Sci.* 7 (2014) 867–884.
- [25] Y. Bar-Cohen, *Electroactive Polymer (EAP) Actuators as Artificial Muscles: Reality, Potential, and Challenges* (2nd Edition), SPIE press, Bellingham, WA, 2004.
- [26] M. Shahinpoor, K.J. Kim, Ionic polymer-metal composites: I. Fundamentals, *Smart Mater. Struct.* 10 (2001) 819.
- [27] R. Baughman, L. Shacklette, R. Elsenbaumer, E. Plichta, C. Becht, Conducting polymer electromechanical actuators, in: *Conjugated Polymeric Materials: Opportunities in Electronics, Optoelectronics, and Molecular Electronics* (J.L. Bredas, R.R. Chance, eds), pp. 559–582, Springer, Dordrecht, 1990.
- [28] E. Smela, Conjugated polymer actuators for biomedical applications, *Adv Mater.* 15 (2003) 481–494.
- [29] R.H. Baughman, C. Cui, A.A. Zakhidov, Z. Iqbal, J.N. Barisci, G.M. Spinks, G.G. Wallace, A. Mazzoldi, D. De Rossi, A.G. Rinzler, O. Jaschinski, S. Roth, M. Kertesz, Carbon Nanotube Actuators, *Science*. 284 (1999) 1340–1344.
- [30] W. Lu, A.G. Fadeev, B. Qi, E. Smela, B.R. Mattes, J. Ding, G.M. Spinks, J. Mazurkiewicz, D. Zhou, G.G. Wallace, Use of ionic liquids for π -conjugated polymer electrochemical devices, *Science*. 297 (2002) 983–987.
- [31] T. Fukushima, A. Kosaka, Y. Ishimura, T. Yamamoto, T. Takigawa, N. Ishii, T. Aida, Molecular ordering of organic molten salts triggered by single-walled carbon nanotubes, *Science*. 300 (2003) 2072–2074.
- [32] T. Fukushima, K. Asaka, A. Kosaka, T. Aida, Fully Plastic Actuator through Layer-by-Layer Casting with Ionic-Liquid-Based Bucky Gel, *Angew Chem Int Ed.* 44 (2005) 2410–2413.
- [33] K. Mukai, K. Asaka, T. Sugino, K. Kiyohara, I. Takeuchi, N. Terasawa, D.N. Futaba, K. Hata, T. Fukushima, T. Aida, Highly Conductive Sheets from Millimeter-Long Single-Walled Carbon Nanotubes and Ionic Liquids: Application to Fast-Moving, Low-Voltage Electromechanical Actuators Operable in Air, *Adv Mater.* 21 (2009) 1582–1585.
- [34] J. Torop, M. Arulepp, J. Leis, A. Punning, U. Johanson, V. Palmre, A. Aabloo, Nanoporous Carbide-Derived Carbon Material-Based Linear Actuators, *Materials*. 3 (2009) 9–25.
- [35] V. Palmre, E. Lust, A. Janes, M. Koel, A. Peikola, J. Torop, U. Johanson, A. Aabloo, Electroactive polymer actuators with carbon aerogel electrodes, *J. Mater. Chem.* 21 (2011) 2577–2583.
- [36] X. Xie, L. Qu, C. Zhou, Y. Li, J. Zhu, H. Bai, G. Shi, L. Dai, An Asymmetrically Surface-Modified Graphene Film Electrochemical Actuator, *ACS Nano*. 4 (2010) 6050–6054.

- [37] M. Ghaffari, W. Kinsman, Y. Zhou, S. Murali, Q. Burlingame, M. Lin, R. Ruoff, Q. Zhang, Aligned Nano-Porous Microwave Exfoliated Graphite Oxide Ionic Actuators with High Strain and Elastic Energy Density, *Adv Mater.* 25 (2013) 6277–6283.
- [38] J. Torop, V. Palmre, M. Arulepp, T. Sugino, K. Asaka, A. Aabloo, Flexible supercapacitor-like actuator with carbide-derived carbon electrodes, *Carbon.* 49 (2011) 3113–3119.
- [39] J. Torop, M. Arulepp, J. Leis, A. Punning, U. Johanson, A. Aabloo, Low voltage linear actuators based on carbide-derived carbon powder, *Proc. SPIE.* 7287 (2009) 72870S-72870S-8.
- [40] P. Simon, P. Taberna, F. Béguin, Electrical Double-Layer Capacitors and Carbons for EDLCs, in: *Supercapacitors: Materials, Systems, and Applications* (E.F. François Béguin, E. Frackowiak, eds), pp. 131–165. Wiley, Weinheim, 2013.
- [41] E.W. Jager, E. Smela, O. Inganäs, Microfabricating conjugated polymer actuators, *Science.* 290 (2000) 1540–1545.
- [42] A. Maziz, C. Plesse, C. Soyer, C. Chevrot, D. Teyssié, E. Cattan, F. Vidal, Demonstrating kHz Frequency Actuation for Conducting Polymer Microactuators, *Adv Funct Mater.* (2014) (Advance Article; DOI:10.1002/ adfm.201400373).
- [43] D. Pugal, K. Jung, A. Aabloo, K.J. Kim, Ionic polymer-metal composite mechano-electrical transduction: review and perspectives, *Polym. Int.* 59 (2010) 279–289.
- [44] Y. Wu, G. Alici, J.D. Madden, G.M. Spinks, G.G. Wallace, Soft Mechanical Sensors Through Reverse Actuation in Polypyrrole, *Adv Funct Mater.* 17 (2007) 3216–3222.
- [45] K. Kruusamäe, P. Brunetto, A. Punning, M. Kodu, R. Jaaniso, S. Graziani, L. Fortuna, A. Aabloo, Electromechanical model for a self-sensing ionic polymer-metal composite actuating device with patterned surface electrodes, *Smart Mater. Struct.* 20 (2011) 124001.
- [46] J.G. Martinez, T.F. Otero, Mechanical awareness from sensing artificial muscles: Experiments and modeling, *Sensor Actuat B-Chem.* 195 (2014) 365–372.
- [47] K. Kruusamäe, A. Punning, A. Aabloo, Electrical Model of a Carbon-Polymer Composite (CPC) Collision Detector, *Sensors.* 12 (2012) 1950–1966.
- [48] S.W. John, G. Alici, C.D. Cook, Towards the position control of conducting polymer trilayer bending actuators with integrated feedback sensor, *IEEE/ASME International Conference on Advanced Intelligent Mechatronics (AIM2009).* 65–70 (2009).
- [49] K. Sadeghipour, R. Salomon, S. Neogi, Development of a novel electrochemically active membrane and 'smart' material based vibration sensor/damper, *Smart Mater. Struct.* 1 (1992) 172.
- [50] U. Zangrilli, L. Weiland, Prediction of the ionic polymer transducer sensing of shear loading, *Smart Mater. Struct.* 20 (2011) 094013.
- [51] B. Kocer, L.M. Weiland, Experimental investigation of the streaming potential hypothesis for ionic polymer transducers in sensing, *Smart Mater. Struct.* 22 (2013) 035020.
- [52] S. Nemat-Nasser, J.Y. Li, Electromechanical response of ionic polymer-metal composites, *J. Appl. Phys.* 87 (2000) 3321–3331.
- [53] K.M. Newbury, D.J. Leo, Linear Electromechanical Model of Ionic Polymer Transducers -Part II: Experimental Validation, *Journal of Intelligent Material Systems and Structures.* 14 (2003) 343–357.

- [54] F. Gao, L.M. Weiland, Ionic polymer transducers in sensing: Implications of the streaming potential hypothesis for varied electrode architecture and loading rate, *J. Appl. Phys.* 108 (2010) 034910–034910–8.
- [55] M.D. Bennett, D.J. Leo, Ionic liquids as stable solvents for ionic polymer transducers, *Sensors and Actuators A: Physical.* 115 (2004) 79–90.
- [56] B.J. Akle, Design of an improved signal conditioning circuit for ionic polymer sensors based on the streaming potential hypothesis, *J Intell Mater Syst Struct.* 24 (2013) 1123–1130.
- [57] W. Takashima, T. Uesugi, M. Fukui, M. Kaneko, K. Kaneto, Mechanochemo-electrical effect of polyaniline film, *Synth. Met.* 85 (1997) 1395–1396.
- [58] G. Alici, G.M. Spinks, J.D. Madden, Y. Wu, G.G. Wallace, Response characterization of electroactive polymers as mechanical sensors, *IEEE/ASME Trans. Mechatronics.* 13 (2008) 187–196.
- [59] T. Shoa, J.D.W. Madden, T. Mirfakhrai, G. Alici, G.M. Spinks, G.G. Wallace, Electromechanical coupling in polypyrrole sensors and actuators, *Sensor Actuat A-Phys.* 161 (2010) 127–133.
- [60] S. John, G. Alici, G.M. Spinks, J. Madden, G. Wallace, Towards fully optimized conducting polymer bending sensors: the effect of geometry, *Smart Mater. Struct.* 18 (2009) 085007.
- [61] T. Mirfakhrai, T. Shoa, N. Fekri, J. Madden, A model for mechanical force sensing in conducting polymers, *ECS Trans.* 28 (2010) 59–71.
- [62] N. Kamamichi, T. Maeba, M. Yamakita, T. Mukai, Printing Fabrication of a Bucky Gel Actuator/Sensor and Its Application to Three-Dimensional Patterned Devices, *Adv. Rob.* 24 (2010) 1471–1487.
- [63] A.K. Ghamsari, Y. Jin, E. Woldesenbet, Mechanical characterization of bucky gel morphing nanocomposite for actuating/sensing applications, *Smart Mater. Struct.* 21 (2012) 045007.
- [64] M. Otsuki, T. Okuyama, M. Tanaka, Time response properties on deformation velocity for a solid polymer electrolyte sensor, *Int. J. Appl. Electromagn. Mech.* 39 (2012) 1063–1068.
- [65] T. Mirfakhrai, Jiyoung Oh, M.E. Kozlov, Shaoli Fang, Mei Zhang, R.H. Baughman, J.D.W. Madden, Mechano-electrical Force Sensors Using Twisted Yarns of Carbon Nanotubes, *IEEE/ASME Trans. Mechatronics.* 16 (2011) 90–97.
- [66] E.G. Bakhoun, M.H.M. Cheng, Miniature Moisture Sensor Based on Ultracapacitor Technology, *IEEE Trans. Compon. Packag. Manuf. Technol.* 2 (2012) 1151–1157.
- [67] R. Tiwari, K. Kim, IPMC as a mechano-electric energy harvester: tailored properties, *Smart Mater. Struct.* 22 (2013) 015017.
- [68] M. Aureli, C. Prince, M. Porfiri, S.D. Peterson, Energy harvesting from base excitation of ionic polymer metal composites in fluid environments, *Smart Mater. Struct.* 19 (2010) 015003.
- [69] F. Cellini, Y. Cha, M. Porfiri, Energy harvesting from fluid-induced buckling of ionic polymer metal composites, *J Intell Mater Syst Struct.* (2014) (Advance article; DOI:10.1177/1045389X13508333).
- [70] Y. Cha, L. Shen, M. Porfiri, Energy harvesting from underwater torsional vibrations of a patterned ionic polymer metal composite, *Smart Mater. Struct.* 22 (2013) 055027.

- [71] M.D. Bennett, D.J. Leo, G.L. Wilkes, F.L. Beyer, T.W. Pechar, A model of charge transport and electromechanical transduction in ionic liquid-swollen Nafion membranes, *Polymer*. 47 (2006) 6782–6796.
- [72] S. Li, J. Yuan, H. Lipson, Ambient wind energy harvesting using cross-flow fluttering, *J. Appl. Phys.* 109 (2011) 026104.
- [73] K. Kikuchi, S. Tsuchitani, Effects of environmental humidity on electrical properties of ionic polymer-metal composite with ionic liquid, in *ICCAS-SICE (2009)* 4747–4751.
- [74] Z. Chen, X. Tan, A. Will, C. Ziel, A dynamic model for ionic polymer-metal composite sensors, *Smart Mater. Struct.* 16 (2007) 1477.
- [75] K. Krishen, Space applications for ionic polymer-metal composite sensors, actuators, and artificial muscles, *Acta Astronaut.* 64 (2009) 1160–1166.
- [76] F. Kaasik, I. Must, E. Lust, M. Jürgens, V. Presser, A. Punning, R. Temmer, R. Kiefer, A. Aabloo, In situ measurements with CPC micro-actuators using SEM, (2014) 90562B-90562B-8.
- [77] S.J. Kim, I.T. Lee, H. Lee, Y.H. Kim, Performance improvement of an ionic polymer-metal composite actuator by parylene thin film coating, *Smart Mater. Struct.* 15 (2006) 1540.
- [78] S. Naficy, N. Stoboi, P.G. Whitten, G.M. Spinks, G.G. Wallace, Evaluation of encapsulating coatings on the performance of polypyrrole actuators, *Smart Mater. Struct.* 22 (2013) 075005.
- [79] J. Ranke, A. Othman, P. Fan, A. Müller, Explaining Ionic Liquid Water Solubility in Terms of Cation and Anion Hydrophobicity, *International Journal of Molecular Sciences*. 10 (2009) 1271–1289.
- [80] Y. Cao, Y. Chen, X. Sun, Z. Zhang, T. Mu, Water sorption in ionic liquids: kinetics, mechanisms and hydrophilicity, *Phys. Chem. Chem. Phys.* 14 (2012) 12252–12262.
- [81] A.C. MacMillan, T.M. McIntire, J.A. Freites, D.J. Tobias, S.A. Nizkorodov, Interaction of Water Vapor with the Surfaces of Imidazolium-Based Ionic Liquid Nanoparticles and Thin Films, *J Phys Chem B*. 116 (2012) 11255–11265.
- [82] F.D. Francesco, N. Calisi, M. Creatini, B. Melai, P. Salvo, C. Chiappe, Water sorption by anhydrous ionic liquids, *Green Chem.* 13 (2011) 1712–1717.
- [83] E. Lee, J. Rabaey, D. Blaauw, P. Dutta, K. Fu, C. Guestrin, B. Hartmann, R. Jafari, D. Jones, J. Kubiatowicz, The Swarm at the Edge of the Cloud, *IEEE Des Test*, (2014) (Advance article; DOI:10.1109/MDAT.2014.2314600)
- [84] D. Bol, J. De Vos, C. Hocquet, F. Botman, F. Durvaux, S. Boyd, D. Flandre, J. Legat, SleepWalker: A 25-MHz 0.4-V Sub-7-Microcontroller in 65-nm LP/GP CMOS for Low-Carbon Wireless Sensor Nodes, *IEEE J Solid-State Circuits*. 48 (2013) 20–32.
- [85] Z.L. Wang, W. Wu, Nanotechnology-Enabled Energy Harvesting for Self-Powered Micro-/Nanosystems, *Angew Chem Int Ed*. 51 (2012) 11700–11721.
- [86] Z. Li, Z.L. Wang, Air/Liquid-Pressure and Heartbeat-Driven Flexible Fiber Nanogenerators as a Micro/Nano-Power Source or Diagnostic Sensor, *Adv Mater*. 23 (2011) 84–89.
- [87] C.B. Vining, An inconvenient truth about thermoelectrics, *Nat Mater*. 8 (2009) 83–85.
- [88] R. Vullers, R. van Schaijk, I. Doms, C. Van Hoof, R. Mertens, Micropower energy harvesting, *Solid State Electron*. 53 (2009) 684–693.

- [89] C. Sun, J. Shi, D.J. Bayerl, X. Wang, PVDF microbelts for harvesting energy from respiration, *Energy Environ Sci.* 4 (2011) 4508–4512.
- [90] LTC3108 Ultralow Voltage Step-Up Converter and Power Manager, Linear Technology. Web resource, <http://www.linear.com/product/LTC3108> (accessed: 09/05/2014).
- [91] M. Olsson, G.L. Wick, J.D. Isaacs, Salinity gradient power: utilizing vapor pressure differences, *Science.* 206 (1979) 452–454.
- [92] D. Brogioli, R. Zhao, P. Biesheuvel, A prototype cell for extracting energy from a water salinity difference by means of double layer expansion in nanoporous carbon electrodes, *Energy environ sci.* 4 (2011) 772–777.
- [93] S. – Lin, A.P. – Straub, M. – Elimelech, – Thermodynamic Limits of Extractable Energy by Pressure Retarded Osmosis, *Energy Environ Sci.* (2014) (Advance article, DOI: 10.1039/C4EE01020E).
- [94] E. Reyssat, L. Mahadevan, Hygromorphs: from pine cones to biomimetic bilayers, *J R Soc Interface.* 6 (2009) 951–957.
- [95] E. Reyssat, L. Mahadevan, How wet paper curls, *Europhys Lett.* 93 (2011) 54001.
- [96] D.P. Holmes, M. Roché, T. Sinha, H.A. Stone, Bending and twisting of soft materials by non-homogenous swelling, *Soft Matter.* 7 (2011) 5188–5193.
- [97] Y. Ma, Y. Zhang, B. Wu, W. Sun, Z. Li, J. Sun, Polyelectrolyte Multilayer Films for Building Energetic Walking Devices, *Angew Chem.* 123 (2011) 6378–6381.
- [98] S. Lee, J.H. Prosser, P.K. Purohit, D. Lee, Bioinspired Hygromorphic Actuator Exhibiting Controlled Locomotion, *ACS Macro Lett.* 2 (2013) 960–965.
- [99] H. Okuzaki, T. Kuwabara, T. Kunugi, A polypyrrole rotor driven by sorption of water vapour, *Polymer.* 38 (1997) 5491–5492.
- [100] H. Okuzaki, K. Hosaka, H. Suzuki, T. Ito, Humido-sensitive conducting polymer films and applications to linear actuators, *React Funct Polym.* 73 (2013) 986–992.
- [101] M. Ma, L. Guo, D.G. Anderson, R. Langer, Bio-Inspired Polymer Composite Actuator and Generator Driven by Water Gradients, *Science.* 339 (2013) 186–189.
- [102] X. Chen, L. Mahadevan, A. Driks, O. Sahin, Bacillus spores as building blocks for stimuli-responsive materials and nanogenerators, *Nat nanotechnol.* 9 (2014) 137–141.
- [103] Y. Yang, J. Liu, Micro/nanofluidics-enabled energy conversion and its implemented devices, *Front Energy.* 5 (2011) 270–287.
- [104] van der Heyden, Frank HJ, D.J. Bonthuis, D. Stein, C. Meyer, C. Dekker, Power generation by pressure-driven transport of ions in nanofluidic channels, *Nano lett.* 7 (2007) 1022–1025.
- [105] C. Chang, R. Yang, Electrokinetic energy conversion efficiency in ion-selective nanopores, *Appl. Phys. Lett.* 99 (2011) 083102–083102–3.
- [106] R.T. Borno, J.D. Steinmeyer, M.M. Maharbiz, Charge-pumping in a synthetic leaf for harvesting energy from evaporation-driven flows, *Appl. Phys. Lett.* 95 (2009) 013705–013705–3.
- [107] D. Trivedi, C.D. Rahn, W.M. Kier, I.D. Walker, Soft robotics: Biological inspiration, state of the art, and future research, *Appl Bionics Biomech.* 5 (2008) 99–117.
- [108] A. Punning, M. Kruusmaa, A. Aabloo, A self-sensing ion conducting polymer metal composite (IPMC) actuator, *Sensor Actuat A-Phys.* 136 (2007) 656–664.

- [109] S. Trasatti, E. Lust, The potential of zero charge, *Modern Aspect Electrochem.* 33 (1999) 1–215.
- [110] S. Liu, W. Liu, Y. Liu, J. Lin, X. Zhou, M.J. Janik, R.H. Colby, Q. Zhang, Influence of imidazolium-based ionic liquids on the performance of ionic polymer conductor network composite actuators, *Polym. Int.* 59 (2010) 321–328.
- [111] Y. Liu, M. Ghaffari, R. Zhao, J. Lin, M. Lin, Q. Zhang, Enhanced Electromechanical Response of Ionic Polymer Actuators by Improving Mechanical Coupling between Ions and Polymer Matrix, *Macromolecules.* 45 (2012) 5128–5133.
- [112] N. Terasawa, I. Takeuchi, K. Mukai, K. Asaka, The effects of Li salts on the performance of a polymer actuator based on single-walled carbon nanotube-ionic liquid gel, *Polymer.* 51 (2010) 3372–3376.
- [113] F. Kaasik, T. Tamm, M. Hantel, E. Perre, A. Aabloo, E. Lust, M. Bazant, V. Presser, Anisometric Charge Dependent Swelling of Porous Carbon in an Ionic Liquid, *Electrochem Commun.* 34 (2013) 196–199.
- [114] M.M. Hantel, V. Presser, R. Kötz, Y. Gogotsi, In situ electrochemical dilatometry of carbide-derived carbons, *Electrochem Commun.* 13 (2011) 1221–1224.
- [115] L.L. Zhang, Y. Gu, G. Zhao, Advanced Porous Carbon Electrodes for Electrochemical Capacitors, *J.Mater.Chem.A.* 1 (2013) 9395–9408.
- [116] L. Borchardt, M. Oschatz, S. Kaskel, Tailoring porosity in carbon materials for supercapacitor applications, *Mater.Horiz.* 1 (2013) 157–168.
- [117] S. Osswald, C. Portet, Y. Gogotsi, G. Laudisio, J. Singer, J. Fischer, V. Sokolov, J. Kukushkina, A. Kravchik, Porosity control in nanoporous carbide-derived carbon by oxidation in air and carbon dioxide, *J Solid State Chem.* 182 (2009) 1733–1741.
- [118] J. Leis, M. Arulepp, A. Kuura, M. Lätt, E. Lust, Electrical double-layer characteristics of novel carbide-derived carbon materials, *Carbon.* 44 (2006) 2122–2129.
- [119] S. Porada, L. Weinstein, R. Dash, A. Van der Wal, M. Bryjak, Y. Gogotsi, P. Biesheuvel, Water desalination using capacitive deionization with microporous carbon electrodes, *ACS appl mater interfaces.* 4 (2012) 1194–1199.
- [120] M. Oschatz, E. Kockrick, M. Rose, L. Borchardt, N. Klein, I. Senkovska, T. Freudenberg, Y. Korenblit, G. Yushin, S. Kaskel, A cubic ordered, mesoporous carbide-derived carbon for gas and energy storage applications, *Carbon.* 48 (2010) 3987–3992.
- [121] H. Bae, H. Choi, J. Jeong, D. Lim, The effect of reaction temperature on the tribological behavior of the surface modified silicon carbide by the carbide derived carbon process, *Mater. Manuf. Process.* 25 (2010) 345–349.
- [122] A. Erdemir, A. Kovalchenko, M. McNallan, S. Welz, A. Lee, Y. Gogotsi, B. Carroll, Effects of high-temperature hydrogenation treatment on sliding friction and wear behavior of carbide-derived carbon films, *Surf Coat Tech.* 188 (2004) 588–593.
- [123] J. Chmiola, C. Largeot, P. Taberna, P. Simon, Y. Gogotsi, Monolithic Carbide-Derived Carbon Films for Micro-Supercapacitors, *Science.* 328 (2010) 480–483.
- [124] P. Huang, M. Heon, D. Pech, M. Brunet, P. Taberna, Y. Gogotsi, S. Lofland, J.D. Hettinger, P. Simon, Micro-supercapacitors from carbide derived carbon (CDC) films on silicon chips, *J. Power Sources.* 225 (2013) 240–244.
- [125] S. Osswald, J. Chmiola, Y. Gogotsi, Structural evolution of carbide-derived carbons upon vacuum annealing, *Carbon.* 50 (2012) 4880–4886.

- [126] F.W. Richey, B. Dyatkin, Y. Gogotsi, Y.A. Elabd, Ion Dynamics in Porous Carbon Electrodes in Supercapacitors Using in Situ Infrared Spectroelectrochemistry, *J. Am. Chem. Soc.* 135 (2013) 12818–12826.
- [127] F. Endres, S.Z. El Abedin, Air and water stable ionic liquids in physical chemistry, *Phys Chem Chem Phys.* 8 (2006) 2101–2116.
- [128] O. Cabeza, S. García-Garabal, L. Segade, M. Domínguez-Pérez, E. Rilo, L.M. Varela, Physical Properties of Binary Mixtures of ILs with Water and Ethanol. A Review, in: *Ionic Liquids Theory, properties, new approaches* (A. Kokorin, Ed), pp 111–136, InTech Press, 2011.
- [129] E. Rilo, J. Vila, J. Pico, S. García-Garabal, L. Segade, L.M. Varela, O. Cabeza, Electrical Conductivity and Viscosity of Aqueous Binary Mixtures of 1-Alkyl-3-methyl Imidazolium Tetrafluoroborate at Four Temperatures, *J Chem Eng Data.* 55 (2009) 639–644.
- [130] A. Jarosik, S.R. Krajewski, A. Lewandowski, P. Radzimski, Conductivity of ionic liquids in mixtures, *J Mol Liq.* 123 (2006) 43–50.
- [131] M.C. Buzzeo, C. Hardacre, R.G. Compton, Use of Room Temperature Ionic Liquids in Gas Sensor Design, *Anal. Chem.* 76 (2004) 4583–4588.
- [132] C. Liang, C. Yuan, R.J. Warmack, C.E. Barnes, S. Dai, Ionic liquids: a new class of sensing materials for detection of organic vapors based on the use of a quartz crystal microbalance, *Anal. Chem.* 74 (2002) 2172–2176.
- [133] H. Tokuda, S. Tsuzuki, Susan, Md Abu Bin Hasan, K. Hayamizu, M. Watanabe, How ionic are room-temperature ionic liquids? An indicator of the physicochemical properties, *J Phys Chem B.* 110 (2006) 19593–19600.
- [134] A. Stoppa, J. Hunger, R. Buchner, Conductivities of Binary Mixtures of Ionic Liquids with Polar Solvents, *J Chem Eng Data.* 54 (2008) 472–479.
- [135] Y. Yu, A.N. Soriano, M. Li, Heat capacities and electrical conductivities of 1-ethyl-3-methylimidazolium-based ionic liquids, *J Chem Thermodyn.* 41 (2009) 103–108.
- [136] P. Lin, A.N. Soriano, R.B. Leron, M. Li, Measurements and correlations of electrolytic conductivity and molar heat capacity for the aqueous ionic liquid systems containing [Emim][EtSO₄] or [Emim][CF₃SO₃], *Exp. Therm. Fluid Sci.* 35 (2011) 1107–1112.
- [137] X. Zhang, L. Lu, Y. Cai, Surface Properties of Ionic Liquid Adsorbate Layer Are Influenced by the Dipole of the Underneath Substrate, *Langmuir.* 28 (2012) 9593–9600.
- [138] S. Imaizumi, Y. Kato, H. Kokubo, M. Watanabe, Driving mechanisms of ionic polymer actuators having electric double layer capacitor structures, *J Phys Chem B.* 116 (2012) 5080–5089.
- [139] S. Sekhon, J. Park, E. Cho, Y. Yoon, C. Kim, W. Lee, Morphology studies of high temperature proton conducting membranes containing hydrophilic/ hydrophobic ionic liquids, *Macromolecules.* 42 (2009) 2054–2062.
- [140] B.J. Akle, M.D. Bennett, D.J. Leo, High-strain ionomeric-ionic liquid electroactive actuators, *Sensor Actuat A-Phys.* 126 (2006) 173–181.
- [141] P.J. James, J.A. Elliott, T.J. McMaster, J.M. Newton, A.M.S. Elliott, S. Hanna, M.J. Miles, Hydration of Nafion® studied by AFM and X-ray scattering, *J Mater Sci.* 35 (2000) 5111–5119.
- [142] L.M. Onishi, J.M. Prausnitz, J. Newman, Water-Nafion Equilibria. Absence of Schroeder's Paradox, *J Phys Chem B.* 111 (2007) 10166–10173.

- [143] F. Tailoka, D. Fray, R. Kumar, Application of Nafion electrolytes for the detection of humidity in a corrosive atmosphere, *Solid State Ionics*. 161 (2003) 267–277.
- [144] L. Sun, T. Okada, Simultaneous determination of the concentration of methanol and relative humidity based on a single Nafion(Ag)-coated quartz crystal microbalance, *Anal. Chim. Acta*. 421 (2000) 83–92.
- [145] B. Akle, S. Nawshin, D. Leo, Reliability of high strain ionomeric polymer transducers fabricated using the direct assembly process, *Smart Mater. Struct.* 16 (2007) S256.
- [146] J. Hou, Z. Zhang, L.A. Madsen, Cation/anion associations in ionic liquids modulated by hydration and ionic medium, *J Phys Chem B*. 115 (2011) 4576–4582.
- [147] D. Mecerreyes, Polymeric ionic liquids: Broadening the properties and applications of polyelectrolytes, *Prog Polym Sci*. 36 (2011) 1629–1648.
- [148] B.J. Akle, M.D. Bennett, D.J. Leo, K.B. Wiles, J.E. McGrath, Direct assembly process: a novel fabrication technique for large strain ionic polymer transducers, *J. Mater. Sci.* 42 (2007) 7031–7041.
- [149] V. Palmre, D. Brandell, U. Mäeorg, J. Torop, O. Volobujeva, A. Punning, U. Johanson, M. Kruusmaa, A. Aabloo, Nanoporous carbon-based electrodes for high strain ionomeric bending actuators, *Smart Mater. Struct.* 18 (2009) 095028.
- [150] J. Torop, F. Kaasik, T. Sugino, A. Aabloo, K. Asaka, Electromechanical characteristics of actuators based on carbide-derived carbon, *Proc.SPIE*. 7642 (2010) 76422A.
- [151] I. Must, F. Kaasik, I. Põldsalu, U. Johanson, A. Punning, A. Aabloo, A carbide-derived carbon laminate used as a mechanoelectrical sensor, *Carbon*. 50 (2012) 535–541.
- [152] M.G. Freire, C.M.S.S. Neves, I.M. Marrucho, J.A.P. Coutinho, A.M. Fernandes, Hydrolysis of Tetrafluoroborate and Hexafluorophosphate Counter Ions in Imidazolium-Based Ionic Liquids, *J Phys Chem A*. 114 (2009) 3744–3749.
- [153] A. Hunt, Z. Chen, X. Tan, M. Kruusmaa, Feedback control of a coupled IPMC (ionic polymer-metal composite) sensor-actuator, *ASME 2009 Dynamic Systems and Control Conference*. (2009) 485–491.
- [154] P. Brunetto, L. Fortuna, P. Giannone, S. Graziani, F. Pagano, A resonant vibrating tactile probe for biomedical applications based on IPMC, *IEEE Trans. Instrum. Meas.* 59 (2010) 1453–1462.
- [155] J. Tao, X.B. Yu, Hair flow sensors: from bio-inspiration to bio-mimicking – a review, *Smart Mater. Struct.* 21 (2012) 113001.
- [156] J. Parcell, N. Aydemir, H. Devaraj, J. Travas-Sejdic, D. Williams, K. Aw, A novel air flow sensor from printed PEDOT micro-hairs, *Smart Mater. Struct.* 22 (2013) 112001.
- [157] C. Bonomo, L. Fortuna, P. Giannone, S. Graziani, A method to characterize the deformation of an IPMC sensing membrane, *Sensor Actuat A-Phys.* 123–124 (2005) 146–154.
- [158] K. Farinholt, D.J. Leo, Modeling of electromechanical charge sensing in ionic polymer transducers, *Mech. Mater.* 36 (2004) 421–433.
- [159] C. Bonomo, L. Fortuna, P. Giannone, S. Graziani, S. Strazzeri, A model for ionic polymer metal composites as sensors, *Smart Mater. Struct.* 15 (2006) 749.
- [160] B. Paola, L. Fortuna, P. Giannone, S. Graziani, S. Strazzeri, IPMCs as Vibration Sensors, *IEEE Instrumentation and Measurement Technology Conference (IMTC 2008)*. 2065–2069 (2008).

- [161] E. Biddiss, T. Chau, Electroactive polymeric sensors in hand prostheses: Bending response of an ionic polymer metal composite, *Med. Eng. Phys.* 28 (2006) 568–578.
- [162] A. Punning, M. Kruusmaa, A. Aabloo, Surface resistance experiments with IPMC sensors and actuators, *Sensor Actuat A-Phys.* 133 (2007) 200–209.
- [163] M. Otsuki, T. Okuyama, M. Tanaka, Characterization of a curvature sensor using a solid polymer electrolyte, *ICMIT 2009: Mechatronics and Information Technology*. International Society for Optics and Photonics. 7500 (2009).
- [164] D.L. Hung, X. Yang, G. Zhu, T. Ganley, X. Tan, Modeling of Ionic Polymer-Metal Composite beam dynamics and its validation using high-speed motion visualization, *Advanced Intelligent Mechatronics (AIM)*, 2010 IEEE/ASME International Conference on. (2010) 175–180.
- [165] K. Farinholt, D.J. Leo, Modeling of electromechanical charge sensing in ionic polymer transducers, *Mech. Mater.* 36 (2004) 421–433.
- [166] L. Greenspan, Humidity fixed points of binary saturated aqueous solutions, *J. Res. Natl. Bur. Stand.* 81 (1977) 89–96.
- [167] I. Takeuchi, K. Asaka, K. Kiyohara, T. Sugino, K. Mukai, H. Randriamahazaka, Electrochemical Impedance Spectroscopy and Electromechanical Behavior of Bucky-Gel Actuators Containing Ionic Liquids, *J Phys Chem C.* 114 (2010) 14627–14634.

ACKNOWLEDGEMENTS

I would like to express my sincere gratitude to my advisors, Prof. Alvo Aabloo and Dr. Andres Punning, for their support and valuable guidance in reaching an important milestone on the *Publish-Or-Perish*-field of *academia*. I highly value the supportive and friendly working atmosphere created by all of my colleagues in the IMS lab. In particular, I highly value the fruitful scientific conversations, estimatedly weeks long if put in one row, held with Urmas Johanson on various aspects of electrochemistry. I highly acknowledge the important contribution by Friedrich Kaasik and Inga Põldsalu in preparation of the IEAP materials used in this work. Prof. E. Lust from the Institute of Chemistry at University of Tartu is acknowledged for providing the porosity measurements of the CDC materials. I appreciate Anna-Liisa Peikolainen and Karl Kruusamäe for proofreading this thesis.

My special thanks to Sigrid, to my mother, and to my other relatives for their continual support.

This work has been financially supported by the Estonian Science Foundation grant nos. 7811 and 8553; by targeted financing SF0180008s08 from the Estonian Ministry of Education; by Institutional Research Funding project IUT20-24 from the Estonian Research Council; by the Tiger University Program of the Information Technology Foundation for Education; by the European Social Fund's (ESF) Doctorial Studies and Internationalisation Programme DoRa, which is carried out by Foundation Archimedes; by the national scholarship program Kristjan Jaak, which is funded and managed by Foundation Archimedes in collaboration with the Ministry of Education and Research; by the Estonian Doctoral School in Information and Communication Technology; and by the graduate school "Functional materials and technologies".

PUBLICATIONS

CURRICULUM VITAE

Name: Indrek Must
Date of birth: 30.04.1985
Phone: +372 5564 2233
E-mail: indrekm@ut.ee

Education:

2009 onwards University of Tartu, Faculty of Science and Technology, doctoral studies in Engineering and Technology
2007–2009 University of Tartu, Faculty of Science and Technology, MSc in Natural Sciences (Materials Science), *cum laude*
2004–2007 University of Tartu, Faculty of Science and Technology, BSc in Natural Sciences (Materials Science)
2001–2004 Tartu Hugo Treffner Gymnasium

Employment:

2012 onwards University of Tartu, Specialist in Materials Technology

Honors & Awards:

2009 Estonian Academy of Sciences: Students' research II prize

Teaching:

2010–2014 Instructor in the course 'Practical Works in Computer Hardware', University of Tartu
2011–2012 Instructor in the course 'Practical Training' for Bachelor program in Technotronics in Estonian University of Life Sciences, University of Tartu
2012–2014 Tutoring of five bachelor students to completion

Publications (in addition to the four publications included in this thesis):

a) Journal articles:

- Must, I., Kaasik, F., Põldsalu, I., Mihkels, L., Johanson, U., Punning, A. & Aabloo, A. (2014) **Ionic and Capacitive Artificial Muscle for Biomimetic Soft Robotics**, *Advanced Engineering Materials*. *Ahead-of-print*; DOI: 10.1002/adem.201400246.
- Punning, A., Must, I., Põldsalu, I. Vunder, V., Temmer, R., Kruusamäe, K., Kaasik, F., Torop, J., Rinne, P., Lulla, T., Johanson, U., Tamm, T. & Aabloo, A. (2014) **Lifetime measurements of ionic electroactive polymer actuators**, *Journal of Intelligent Material Systems and Structures*, accepted manuscript.
- Kiefer, R., Aydemir, N., Torop, J., Tamm, T., Temmer, R., Travas-Sejdic, J., Must, I., Kaasik, F. & Aabloo, A. (2014) **Carbide-derived carbon as active interlayer of polypyrrole tri-layer linear actuator**, *Sensors & Actuators: B. Chemical*, **201**, 100–106.

Temmer, R., Must, I., Kaasik, F., Aabloo, A. & Tamm, T. (2012) **Combined chemical and electrochemical synthesis methods for metal-free polypyrrole actuators**, *Sensors and Actuators B: Chemical*, **166**, 411–418.

b) Full papers in Conference Proceedings:

Must, I., Kaasik, F., Põldsalu, I., Mihkels, L., Johanson, U., Punning, A. & Aabloo, A. (2014) **Pulse-Width-Modulated Charging of Ionic and Capacitive Actuators**, 2014 IEEE/ASME International Conference on Advanced Intelligent Mechatronics (AIM2014), 1446–1451.

Kaasik, F., Must, I., Lust, E., Jürgens, M., Presser, V., Punning, A., Temmer, R., Kiefer, R. & Aabloo, A. (2014) **In situ measurements with CPC micro-actuators using SEM**, *Proceedings of SPIE*, **9056**, 90562B.

Tamm, T., Pärilin, K., Tiimus, T., Leemets, K., Terasmaa, T. & Must, I. **Smart insole sensors for sports and rehabilitation**, *Proceedings of SPIE*, **9060**, 90600L.

Must, I., Johanson, U., Kaasik, F., Põldsalu, I., Punning, A. & Aabloo, A. (2013) **An ionic liquid-based actuator as a humidity sensor**, IEEE/ASME International Conference on Advanced Intelligent Mechatronics (AIM2013), 1498–1503.

Must, I., Kaasik, F., Põldsalu, I., Johanson, U., Punning, A. & Aabloo, A. (2012) **Carbon-polymer-ionic liquid composite as a motion sensor**, *Proceedings of SPIE*, **8340**, 834019.

Kaasik, F., Torop, J., Must, I., Soolo, E., Põldsalu, I., Peikolainen, A.L., Palmre, V. & Aabloo, A. (2012). **Ionic EAP transducers with amorphous nanoporous carbon electrodes**, *Proceedings of SPIE*, **8340**, 83400V.

Must, I., Kruusamäe, K.; Johanson, U.; Tamm, T.; Punning, A. & Aabloo, A. (2011). **Characterisation of electromechanically active polymers using electrochemical impedance spectroscopy**, in *Lecture Notes on Impedance Spectroscopy: Measurement, Modeling and Applications 2*, Kanoun, O. (Ed.), CRC press, 113–121.

Must, I., Anton, M., Kruusmaa, M. & Aabloo, A. (2009) **Linear modeling of elongated bending EAP actuator at large deformations**, *Proceedings of SPIE*, **7287**, 728723.

c) Inventions:

Differential electrochemically active humidity sensor and its use as energy storage or energy collection device; Owner: University of Tartu; Authors: Indrek Must, Urmas Johanson, Inga Põldsalu, Andres Punning, Alvo Aabloo, Friedrich Kaasik; Priority number: P201300001; Priority date: 30.01.2013

A sensor material; Owner: University of Tartu; Authors: Indrek Must, Urmas Johanson, Andres Punning, Alvo Aabloo, Inga Põldsalu, Friedrich Kaasik; Priority number: P201100015; Priority date: 05.03.2011

ELULOOKIRJELDUS

Nimi: Indrek Must
Sünniaeg: 30.04.1985
Telefon: +372 5564 2233
E-mail: indrekm@ut.ee

Haridustee:

alates 2009 Tartu Ülikool, Loodus- ja Tehnoloogiateaduskond, doktoriõpe
2007–2009 Tartu Ülikool, Loodus- ja Tehnoloogiateaduskond, loodus-
teaduste magister materjaliteaduses, *cum laude*
2004–2007 Tartu Ülikool, Loodus- ja Tehnoloogiateaduskond, loodus-
teaduste bakalaureus materjaliteaduses.
2001–2004 Tartu Hugo Treffneri Gümnaasium

Teenistuskäik:

alates 2012 Tartu Ülikool, materjalitehnoloogia spetsialist

Tunnustused:

2009 Eesti Teaduste Akadeemia: üliõpilaste teadustööde konkursi II auhind

Õppetöö läbiviimine:

2010–2014 Juhendaja õppeaines “Arvutiriistvara praktikum”, Tartu Ülikool
2011–2012 Juhendaja õppeaines “Erialapraktika” Eesti Maaülikooli Tehno-
troonika bakalaureuseõppekava tudengitele, Tartu Ülikool
2012–2014 Juhendaja viiele bakalaureusetööle

Publikatsioonid (lisaks käesolevas doktoritöös sisalduvale neljale publikatsioonile):

a) Ajakirjaartiklid:

Must, I., Kaasik, F., Põldsalu, I., Mihkels, L., Johanson, U., Punning, A. & Aabloo, A. (2014) **Ionic and Capacitive Artificial Muscle for Biomimetic Soft Robotics**, *Advanced Engineering Materials*. Eelavaldatud veebis; DOI: 10.1002/adem.201400246.

Punning, A., Must, I., Põldsalu, I. Vunder, V., Temmer, R., Kruusamäe, K., Kaasik, F., Torop, J., Rinne, P., Lulla, T., Johanson, U., Tamm, T. & Aabloo, A. (2014) **Lifetime measurements of ionic electroactive polymer actuators**, *Journal of Intelligent Material Systems and Structures*, avaldamiseks vastu võetud.

Kiefer, R., Aydemir, N., Torop, J., Tamm, T., Temmer, R., Travas-Sejdic, J., Must, I., Kaasik, F. & Aabloo, A. (2014) **Carbide-derived carbon as active interlayer of polypyrrole tri-layer linear actuator**, *Sensors & Actuators: B. Chemical*, **201**, 100–106.

Temmer, R., Must, I., Kaasik, F., Aabloo, A., & Tamm, T. (2012) **Combined chemical and electrochemical synthesis methods for metal-free polypyrrole actuators**, *Sensors and Actuators B: Chemical*, **166**, 411–418.

b) Kogumikuartiklid:

Must, I., Kaasik, F., Põldsalu, I., Mihkels, L., Johanson, U., Punning, A. & Aabloo, A. (2014) **Pulse-Width-Modulated Charging of Ionic and Capacitive Actuators**, 2014 IEEE/ASME International Conference on Advanced Intelligent Mechatronics (AIM2014), *1446–1451*.

Kaasik, F., Must, I., Lust, E., Jürgens, M., Presser, V., Punning, A., Temmer, R., Kiefer, R., Aabloo, A. (2014) **In situ measurements with CPC micro-actuators using SEM**, *Proceedings of SPIE*, **9056**, 90562B.

Tamm, T., Pärilin, K., Tiimus, T., Leemets, K., Terasmaa, T. & Must, I. **Smart insole sensors for sports and rehabilitation**, *Proceedings of SPIE*, **9060**, 90600L.

Must, I., Johanson, U., Kaasik, F., Põldsalu, I., Punning, A., Aabloo, A. (2013) **An ionic liquid-based actuator as a humidity sensor**, IEEE/ASME International Conference on Advanced Intelligent Mechatronics (AIM2013), 1498–1503.

Must, I., Kaasik, F., Põldsalu, I., Johanson, U., Punning, A., & Aabloo, A. (2012) **Carbon-polymer-ionic liquid composite as a motion sensor**, *Proceedings of SPIE*, **8340**, 834019.

Kaasik, F., Torop, J., Must, I., Soolo, E., Põldsalu, I., Peikolainen, A.L., Palmre, V., Aabloo, A. (2012). **Ionic EAP transducers with amorphous nanoporous carbon electrodes**, *Proceedings of SPIE*, **8340**, 83400V.

Must, I., Kruusamäe, K.; Johanson, U.; Tamm, T.; Punning, A.; Aabloo, A. (2011). **Characterisation of electromechanically active polymers using electrochemical impedance spectroscopy**, *kogumikus Lecture Notes on Impedance Spectroscopy: Measurement, Modeling and Applications 2*, Kanoun, O. (Ed.), CRC press, 113–121.

Must, I., Anton, M., Kruusmaa, M., & Aabloo, A. (2009) **Linear modeling of elongated bending EAP actuator at large deformations**, *Proceedings of SPIE*, **7287**, 728723.

c) Leiutised:

Diferentsiaalne elektroaktiivne niiskusandur ning selle kasutamine energiakogumisest või energiasalvestina; Omanik: Tartu Ülikool; Autorid: Indrek Must, Urmas Johanson, Inga Põldsalu, Andres Punning, Alvo Aabloo, Friedrich Kaasik; Prioriteedinumber: P201300001; Prioriteedikuupäev: 30.01.2013

Sensormaterjal; Omanik: University of Tartu; Authors: Indrek Must, Urmas Johanson, Andres Punning, Alvo Aabloo, Inga Põldsalu, Friedrich Kaasik; Prioriteedinumber: P201100015; Prioriteedikuupäev: 05.03.2011

DISSERTATIONES TECHNOLOGIAE UNIVERSITATIS TARTUENSIS

1. **Imre Mäger.** Characterization of cell-penetrating peptides: Assessment of cellular internalization kinetics, mechanisms and bioactivity. Tartu 2011, 132 p.
2. **Taavi Lehto.** Delivery of nucleic acids by cell-penetrating peptides: application in modulation of gene expression. Tartu 2011, 155 p.
3. **Hannes Luidalepp.** Studies on the antibiotic susceptibility of *Escherichia coli*. Tartu 2012, 111 p.
4. **Vahur Zadin.** Modelling the 3D-microbattery. Tartu 2012, 149 p.
5. **Janno Torop.** Carbide-derived carbon-based electromechanical actuators. Tartu 2012, 113 p.
6. **Julia Suhorutšenko.** Cell-penetrating peptides: cytotoxicity, immunogenicity and application for tumor targeting. Tartu 2012, 139 p.
7. **Viktoryia Shyp.** G nucleotide regulation of translational GTPases and the stringent response factor RelA. Tartu 2012, 105 p.
8. **Mardo Kõivomägi.** Studies on the substrate specificity and multisite phosphorylation mechanisms of cyclin-dependent kinase Cdk1 in *Saccharomyces cerevisiae*. Tartu, 2013, 157 p.
9. **Liis Karo-Astover.** Studies on the Semliki Forest virus replicase protein nsP1. Tartu, 2013, 113 p.
10. **Piret Arukuusk.** NickFects—novel cell-penetrating peptides. Design and uptake mechanism. Tartu, 2013, 124 p.
11. **Piret Villo.** Synthesis of acetogenin analogues. Asymmetric transfer hydrogenation coupled with dynamic kinetic resolution of α -amido- β -keto esters. Tartu, 2013, 151 p.
12. **Villu Kasari.** Bacterial toxin-antitoxin systems: transcriptional cross-activation and characterization of a novel *mqsRA* system. Tartu, 2013, 108 p.
13. **Margus Varjak.** Functional analysis of viral and host components of alphavirus replicase complexes. Tartu, 2013, 151 p.
14. **Liane Viru.** Development and analysis of novel alphavirus-based multi-functional gene therapy and expression systems. Tartu, 2013, 113 p.
15. **Kent Langel.** Cell-penetrating peptide mechanism studies: from peptides to cargo delivery. Tartu, 2014, 115 p.
16. **Rauno Temmer.** Electrochemistry and novel applications of chemically synthesized conductive polymer electrodes. Tartu, 2014, 206 p.